Copyright Warning & Restrictions

The copyright law of the United States (Title 17, United States Code) governs the making of photocopies or other reproductions of copyrighted material.

Under certain conditions specified in the law, libraries and archives are authorized to furnish a photocopy or other reproduction. One of these specified conditions is that the photocopy or reproduction is not to be "used for any purpose other than private study, scholarship, or research." If a, user makes a request for, or later uses, a photocopy or reproduction for purposes in excess of "fair use" that user may be liable for copyright infringement,

This institution reserves the right to refuse to accept a copying order if, in its judgment, fulfillment of the order would involve violation of copyright law.

Please Note: The author retains the copyright while the New Jersey Institute of Technology reserves the right to distribute this thesis or dissertation

Printing note: If you do not wish to print this page, then select "Pages from: first page # to: last page #" on the print dialog screen

NJIT
New Jersey's Science & Technology University

The Van Houten library has removed some of the personal information and all signatures from the approval page and biographical sketches of theses and dissertations in order to protect the identity of NJIT graduates and faculty.

ABSTRACT

DESIGN AND FABRICATION OF OPTICAL RESONATORS

by

Pushkar Moholkar

The design and fabrication of ring optical resonators for high-speed optical communication systems is the topic of this thesis. Its novelty is in two aspects: 1) Use of silicon wafers as an optical guiding medium; 2) Use of wafer bonding technique to attach two optical elements together.

The structure consists of two optical waveguides, the bus waveguide and the drop channel waveguide. A ring on top of these waveguides couples them in such a way that only one narrow spectral line is removed from the bus waveguides which propagates in the drop-channel waveguide. The assembly is fabricated using wafer-bonding technique in silicon. A precise control over the waveguide dimensions, the ring dimensions and the distance between the ring and the waveguide is required for a specific spectral line to be coupled to the drop-channel waveguide. It is hoped that such fabrication techniques will enable the realization of high-speed large bandwidth integrated optical communication and sensor systems.

DESIGN AND FABRICATION OF OPTICAL RESONATORS

by
Pushkar Moholkar

A Thesis
Submitted to the Faculty of
New Jersey Institute of Technology
In Partial Fulfillment of the Requirements for the Degree of
Master of Science in Computer Engineering

Department of Electrical and Computer Engineering

May 2000

APPROVAL PAGE

DESIGN AND FABRICATION OF OPTICAL RESONATORS

Pushkar Moholkar

Dr. Haim Grebel, Thesis Advisor
Professor, NJIT

Date

Dr. Edwin Hou,
Associate Professor, NJIT

Date

Dr. Dentcho Ivanov,
Director, Technical Operations, MERC, NJIT

Date

BIOGRAPHICAL SKETCH

Author: Pushkar Moholkar

Degree: Master of Science in Computer Engineering

Date: May 2000

Undergraduate and Graduate Education:

- Master of Science in Computer Engineering,
  New Jersey Institute of Technology, Newark NJ, 2000
- Bachelor of Engineering in Electronics,
  University of Pune, Pune, India, 1998
- Diploma in Computer Technology,
  Board of Technical Education, Mumbai, India, 1995

Major: Computer Engineering

Dedicated to my parents and my brother

ACKNOWLEDGEMENT

First and foremost, I express my deepest possible gratitude to my thesis advisor Dr. Haim Grebel. He not only helped me technically, but also provided me with the essential insight and motivation to complete my thesis work. I also thank my other committee members Dr. Edwin Hou and Dr. Dentcho Ivanov for actively participating in my thesis committee.

I take this opportunity to thank Dr. Moeller and Dr. Vijayalakshmi for giving valuable suggestions whenever needed. I also thank my fellow graduate student Mr. Mahesh Ajgaonkar for his support. I thank all those who have directly or indirectly contributed in making this thesis a success.

TABLE OF CONTENTS

Chapter	Page
1 INTRODUCTION	1
1.1 Background	1
1.2 Need for Resonators	2
1.3 Basic Optical Resonator	5
1.4 Brief Discussion about this Thesis	5
2 INTRODUCTION TO WAVEGUIDES	7
2.1 Waveguide Structure	7
2.2 Ray Theory Transmission	8
2.2.1 Total Internal Reflection	8
2.2.2 Acceptance Angle	10
2.2.3 Numerical Aperture	11
2.3 Modes in Waveguides	13
2.4 Summary	19
3 DESIGN AND MANUFACTURING OF MASKS	20
3.1 Introduction	20
3.2 Mask for Rectangular Waveguides	20
3.3 Mask for Ring Waveguides	24
3.4 Precautions while Making the Mask	25
3.5 Ordering the Mask	27
4 FABRICATION OF WAVEGUIDES	29

TABLE OF CONTENTS
(Continued)

Chapter **Page**

4.1 Introduction 29

4.2 Process of Fabrication 29

5 EXPERIMENTAL RESULTS 46

5.1 Introduction 46

5.2 Experimental Results 46

6 CONCLUSION AND FUTURE DEVELOPMENTS 53

6.1 Conclusion 53

6.2 Future Developments 53

6.3 Multiple Ring Structure for Better Spectral Filtering 53

REFERENCES 56

LIST OF FIGURES

Figure		Page
1.1	Schematic of a Typical Add/Drop Multiplexer	3
1.2a	Schematic of Optical Resonator	4
1.2b	Cross-section of Optical Resonator	4
2.1	Basic Structure of a Waveguide	8
2.2	Basic Principles of Light Propagation	9
2.3	Transmission of Light through a Perfect Waveguide	11
2.4	Acceptance Angle	11
2.5	Slab Waveguide	14
2.6	Propagation by Multiple Reflection in Planar Waveguide	15
3.1	Top view of Rectangular Waveguide	21
3.2	Structure and Placement of Different Patterns	22
3.3	Schematic of Final Mask	23
3.4	Basic Structure in the Ring Mask	24
3.5	Desired Fracture Window	26
3.6	Image Spill due to Improper Positioning of Pattern	27
4.1	CMOS Grade Silicon Wafer before Bonding	30
4.2	Silicon Wafers with Oxide being Bonded	32
4.3	Bonded Silicon Wafers	33
4.4	Improperly Bonded Wafer	33
4.5	Perfectly Bonded Wafer	34
4.6	Wafer with Nitride and coated with Photoresist	36

LIST OF FIGURES
(Continued)

Figure		Page
4.7	Wafer, after Removing the Oxide and Nitride in the Exposure Area............	37
4.8	Wafer being Etched in KOH Bath..	38
4.9	Wafer being Exposed to UV Rays..	39
4.10	Wafer with Photoresist before M-pyrol..	41
4.11	Wafer after Removal of Photoresist by M-pyrol................................	41
4.12	Profile of Wafer under DEKTAK..	42
4.13	Final Wafer with Oxide..	43
4.14	Wafers before Bonding...	44
4.15	Wafers after Bonding..	44
4.16	Photo of the Waveguide taken through a Microscope............................	45
5.1	Experimental Setup for Measurements of Transmission Characteristics of Waveguide..	47
5.2	Experimental Setup for Verification of the Spectral Output of the Laser Diode..	47
5.3	Output Profile for Laser Light as Input and Horizontal Displacement of Input Launching Fiber.	47
5.4	Output Profile for Laser Light as Input and Vertical Displacement of Input Launching Fiber...	48

LIST OF FIGURES
(Continued)

Figure **Page**

5.5 Transmission Profile for the Waveguide for Different Wavelengths 49

5.6 Experimental Setup for Measurement of the Spectral Characteristics of the Waveguide.. 50

5.7 Transmission Characteristics of Rectangular waveguide with respect to Wavelength.. 51

5.5 Multiple Ring Structure for Better Spectral Filtering 54

CHAPTER 1

INTRODUCTION

1.1 Background

The increasing growth of the Internet and the consequent need for more and more bandwidth has given birth to the new technique called Wavelength Division Multiplexing (WDM). It represents the second major fiber-optic revolution in telecommunications, the first being when, major telecommunication companies replaced copper wires and microwave links with optical fibers. Taking advantage of WDM, long-distance carriers have been able to avoid laying expensive new cables by sending data using additional wavelengths through existing fibers.

Another important development that has occurred in recent years is the first commercial application of integrated-optical devices in analog and digital fiber-optic communication systems and networks. High-speed electro-optic intensity modulators and monolithically integrated electro-absorption modulators, for example, are widely used in long-distance terrestrial and submarine lightwave systems to encode the digital signals with little or no additional frequency-chirp into the optical carriers. Moreover, fast electrooptic polarization scramblers have become an important component in ultra-long transoceanic communication systems to eliminate anisotropic gain saturation in the optical amplifiers. In addition, optical wavelength multiplexers and demultiplexers using silica-based devices are employed in the multi-wavelength communication systems to combine and separate the various optical carriers at the transmitters and receivers. These

applications are just the beginning of an even more widespread commercial use of integrated-optical devices in future long-distance and local area networks.

We discuss the design and manufacturing of integrated optical resonators. These optical resonators have come up.to be the future of Wavelength Division Multiplexing.

1.2 Need for Resonators

The increasing interest in photonic integrated circuits and the increasing use of all optical fiber networks as backbones for global communication systems, has been based in large part on the extremely wide optical transmission bandwidth enabled by optical fibers and the large degree of transparency that they offer. This has accordingly led to an increased demand for the practical utilization of the full optical bandwidth available, which is presently limited by electronic systems. In order to increase the aggregate transmission bandwidth, it is generally preferred that the spacing of simultaneously transmitted optical data streams, or optical data channels on the same optical fiber be closely packed to accommodate a larger number of channels. In other words, the difference in wavelength between two adjacent channels needs to be minimized. Simply put, each channel is characterized by a central optical frequency (central wavelength). Nowadays the spacing between two adjacent channels is 2 nm or 300 GHz. This bandwidth is much larger than the channel bandwidth; the fastest optical communication system is 10 Gb/sec or 5 GHz/sec.

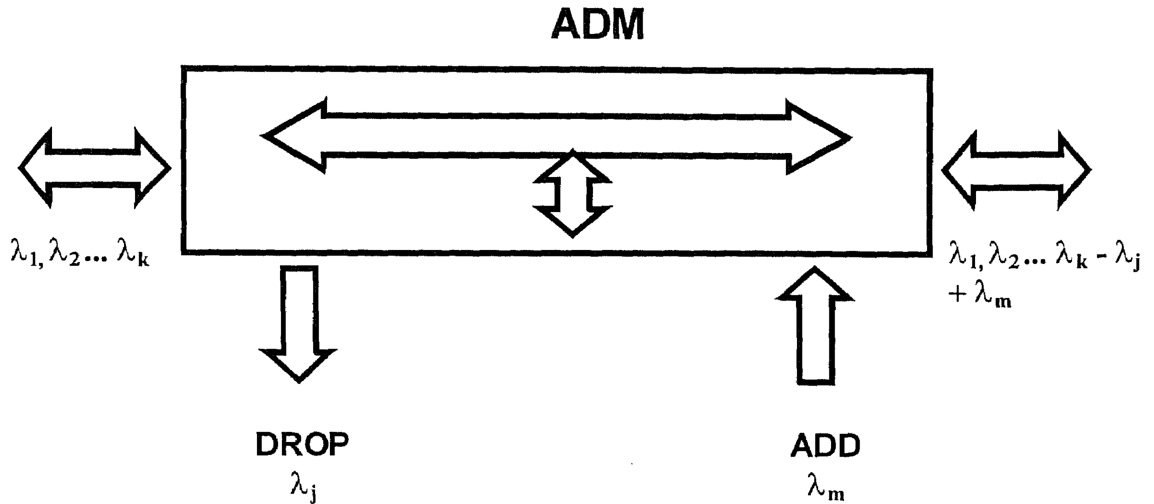

Figure 1.1 Schematic of a Typical Add/Drop Multiplexer

Optical Waveguide Resonators that access one channel of a wavelength division multiplexed signal while leaving other channels undisturbed has become an essential component of photonic integrated circuits and optical communication systems. Among various devices studied recently, resonant filters are attractive candidates for channel dropping because they can potentially be used to select a single channel with a very narrow linewidth accuracy.

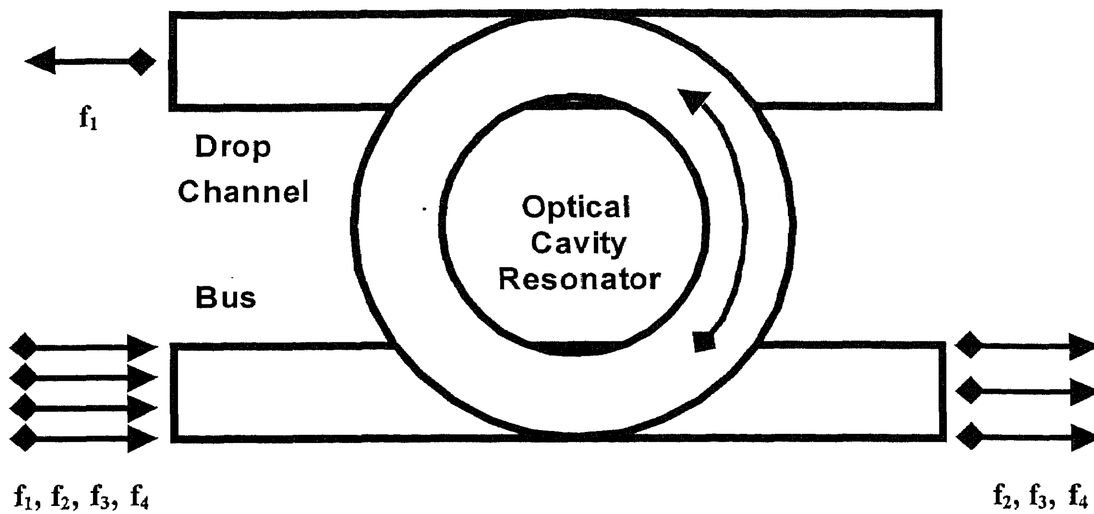

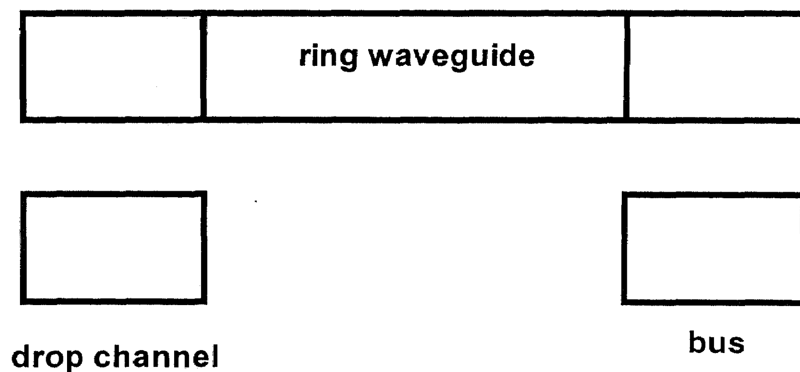

Figure 1.2 a) Schematic of Optical Resonator (top view)

b) Cross Section of Optical Resonator

1.3 Basic Optical Resonator

The schematic of a proposed optical resonator is shown in Fig. 1.1; Two waveguides, the bus and the drop, are coupled through an optical resonator system. While WDM signals (i.e. multi-frequency signals) propagate inside one waveguide (the bus), a single frequency channel is transferred out of the bus and into the other waveguide (the drop) either in the forward or backward propagation direction, while completely prohibiting cross talk between the bus and the drop for all other frequencies.

The performance of an Optical Waveguide Resonator is determined by the transfer efficiency between the two waveguides. Perfect efficiency corresponds to 100% transfer of the selected channel into either the forward or the backward direction in the drop, with no forward transmission or backward reflection into the bus.

In this project, a ring waveguide is used as a resonant filter. In such a geometry, the forward propagating wave in the bus excites a rotating mode in the ring, which in turn couples into the backward propagating mode in the drop. Ideally, at resonance, 100% transfer can be achieved. However, radiation losses and bending losses inside the ring have the effect of reducing the transfer efficiency. Furthermore, the ring waveguides may support multiple resonances, thus in principle may transmit multiple channels.

1.4 Brief Discussion about this Thesis

Our discussion is mainly aimed at the design and fabrication aspects of ring optical resonators. Chapter 2 of this thesis describes the basics of waveguides, different types of waveguides and different parameters of waveguides. Chapter 3 explains the design procedure for optical resonators. Chapter 4 describes the procedure to be followed and

precautions to be taken while designing and drawing the masks for optical resonators. Chapter 5 explains in detail the fabrication procedure for these optical resonators. Chapter 6 gives an idea of the experiments that were carried out on the waveguides. Chapter 7 draws some conclusions from the experimental results. It also explains some future improvements that can be done in the design of these resonators. It also gives some applications for these resonators

CHAPTER 2

INTRODUCTION TO WAVEGUIDES

2.1 Waveguide Structure

A waveguide restricts the three dimensional "free space" propagation of the electromagnetic wave to a single dimension. Usually waveguides are:

- Low loss: That is, the wave travels along the guide without greatly attenuated as it propagates.
- Routable: This means that we can gently bend the guiding structure without losing contact with the wave, without generating reflections, and without incurring additional loss.
- Large spectral bandwidth

There are many different waveguide structures. Usually they are uniform in the direction of propagation of the guided wave, that is, one cannot tell where one is along the waveguide by physically looking around one.

A waveguide structure essentially consists of a core with a refractive index n_1 surrounded by a cladding of slightly lower refractive index n_2. The cladding supports the waveguide structure whilst also, when sufficiently thick, substantially reducing the radiation loss into the surrounding air. In essence, the light energy travels in both the core and the cladding allowing the associated fields to decay to a negligible value at the cladding air interface. Fig 2.1 shows the structure of a cubical waveguide.

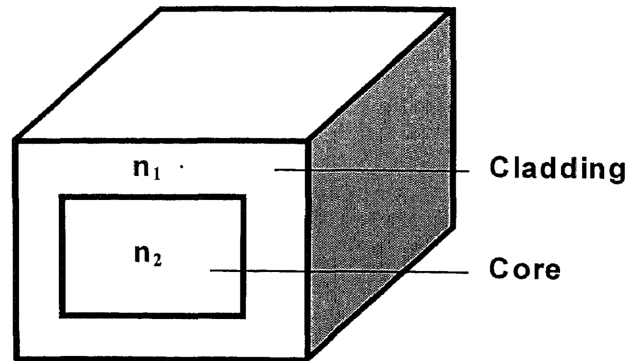

Figure 2.1 Basic Structure of a Waveguide

2.2 Ray Theory Transmission

In the following discussion, we discuss the different parameters of waveguides. We will use the ray theory approach for specifying these parameters.

2.2.1 Total Internal Reflection

For studying the propagation of light within a waveguide using the wave theory, we need to consider the refractive index profile of the material. The refractive index of the medium is defined as the ratio of the velocity of light in vacuum to the velocity of light in the medium. When a ray is incident on the interface between two dielectrics of different refractive indices, refraction occurs. The ray approaching the interface is propagating in a dielectric of refractive index n_1 and at an angle ϕ_1 to the normal at the surface of the interface. If the dielectric on the other side of the interface has a refractive index n_2 which

is less than n_1, then the refraction is such that the ray path in the lower index medium is at an angle ϕ_2 to the normal, where ϕ_2 is greater than ϕ_1. The angle of incidence ϕ_2 and $\phi 1$ are related to each other, and to the refractive indices of the dielectrics by Snell's law of refraction, which states that:

$$n_1 \sin \phi_1 = n_2 \sin \phi_2 \tag{2.1}$$

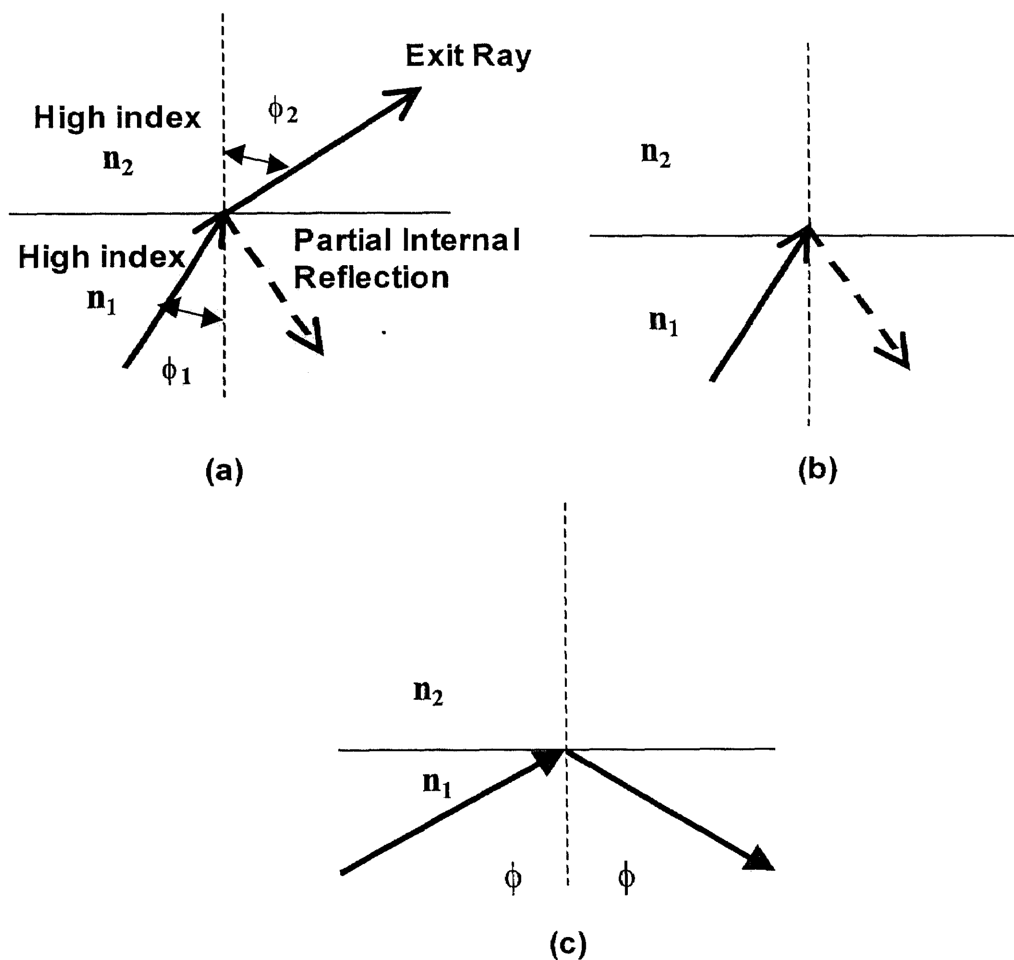

Figure 2.2 Basic Principles of Light Propagation

(a) Refraction (b) the limiting case of refraction showing the critical ray at an angle ϕ_c (c) total internal reflection where $\phi > \phi_c$

A small amount of light is reflected back into the originating reflecting medium (partial internal reflection). As n_1 is greater than n_2, the angle of refraction is always greater than angle of incidence. Thus when the angle of refraction is 90^0 and the refracted ray emerges parallel to the interface between the dielectrics, the angle of incidence must be less than 90^0. This is the limiting case of refraction and this angle of incidence is known as the critical angle ϕc. The value of the critical angle is given by:

$$\sin \varphi_c = \frac{n_2}{n_1} \quad (2.2)$$

At angle of incidence greater than the critical angle, the light is reflected back into the originating dielectric medium (total internal reflection) with high efficiency.

2.2.2 Acceptance Angle:

Fig. 2.3 illustrates a meridional ray A at the critical angle ϕ_c within the waveguide at the core-cladding interface. It may be observed that the ray enters the waveguide core at an angle θ_a to the waveguide axis and is refracted at the air-core interface before transmission to the core-cladding interface at the critical angle. Hence any rays which are incident of the waveguide core at an angle greater than θ_a will be transmitted to the core cladding interface at an angle less than θ_c, and will be totally internally reflected. This situation is illustrated in Fig 2.4, where the incident ray B at an angle greater than θ_a is refracted into the cladding an eventually lost by radiation. Thus, for rays to be transmitted by total internal reflection within the waveguide, they must be incident on the core within an acceptance cone defined by the conical half angle θ_a. Hence θ_a is the maximum angle

to the axis at which light may enter the waveguide in order to be propagated, and is often referred to as the acceptance angle for the waveguide.

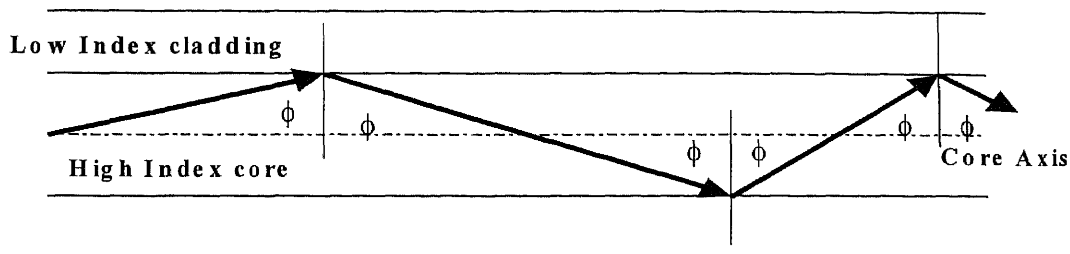

Figure 2.3 Transmission of Light in a Perfect Waveguide

2.2.3 Numerical Aperture:

The ray theory can be used to obtain a relationship between the acceptance angle and the refractive indices of the three media involved, namely the core the cladding and air.

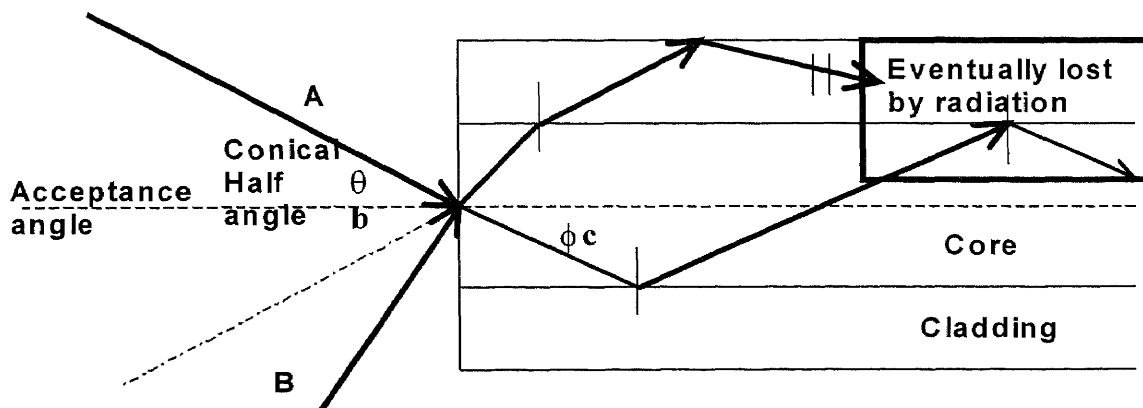

Figure 2.4 Acceptance Angle θ_a when Launching Light into an Optical Fiber

Fig. 2.4 shows a light ray incident on the waveguide core at an angle θ_1 to the waveguide axis which is less than the acceptance angle for the waveguide θ_a. The ray enters the waveguide from a medium (air) of refractive index n_0, and the waveguide core has a refractive index n_1, which is slightly greater than the cladding refractive index n_2. Assuming the entrance face at the waveguide core to be normal to the axis, then considering the refraction at the air-core interface and using Snell's law:

$$n_0 \sin \theta_1 = n_1 \sin \theta_2 \qquad (2.3)$$

We have:

$$\varphi = \frac{\pi}{2} - \theta_2 \qquad (2.4)$$

where ϕ is greater than the critical angle at the core-cladding interface.

Hence, Eq. 2.3 becomes

$$n_0 \sin \theta_1 = n_1 \cos \phi \qquad (2.5)$$

Since $\sin2\ \phi + \cos2\phi = 1$ then

$$n_0 \sin \phi_1 = n_1 (1 - \sin2\phi)^{1/2} \qquad (2.6)$$

When the limiting case for total internal reflection is considered, ϕ becomes equal to the critical angle of the core-cladding interface and is given by Eq. (2.2). Also, in this limiting case θ_1 becomes the acceptance angle of the waveguide θ_a. Combining these limiting cases into Eq. (2.6) gives:

$$n_0 \sin \theta_a = (n_1^2 - n_2^2)^{1/2} \qquad (2.7)$$

The above equation, apart from relating the acceptance angle to the refractive indices, serves as the basis for the definition of the important waveguide parameter, the numerical aperture (NA).

Hence NA is defined as:

$$NA = n_0 \sin \theta_a = (n_1^2 - n_2^2)^{1/2} \quad (2.8)$$

2.3 Modes in Waveguides

We start again with an inner medium guide layer (n_1) and incident on to one of the dielectric surfaces with one of the confining layers (n_2). We assume $n_1 > n_2$. Maxwell's equations require that the transverse components of E and H and the normal components of D and B are continuous across the boundary. From this, several things follow. First and most important are the laws of refraction and total internal reflection we discussed earlier. We saw that these depend on whether the angle of incidence, ϕ is less than or greater than the critical angle ϕ_c. Next is the fact that some reflection occurs even when $\phi < \phi_c$. this is known as Fresnel's reflection. Because of the boundary conditions, the reflection coefficient is different for the components of the fields (E and H) which are parallel to or perpendicular to the interface. Then, when total internal reflection occurs, it is found that there is a phase change at the interface between the incident and reflected waves that varies with the angle of incidence. In terms of the ray model, this means that the reflection appears to take place at the surface lying behind the actual interface, an effect known as Goos-Hanchen shift.

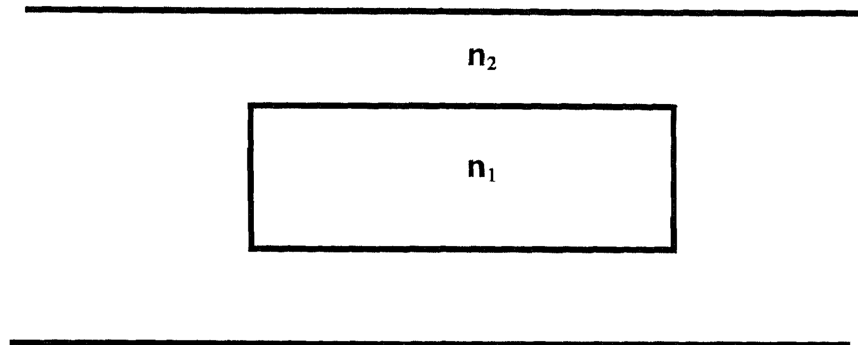

Figure 2.5 Slab Waveguide

Now consider the waveguide shown in Fig. 2.5 in which two such dielectric interfaces are spaced a distance 2d apart. Consider a wave propagating in the guide layer in the positive z-direction. In the ray model, it would progress by multiple reflections as shown in Fig. 2.6. We can think of such a ray as representing a plane TEM wave travelling at an angle θ to the waveguide axis. We see that while the phase velocity in the direction of propagation is

$$v_p = \lambda_m f = \omega/\beta_1 = c.n_1 \quad (2.9)$$

The apparent phase velocity with which the wavefronts intercept any line parallel to the axis is

$$(v_p)_z = (\lambda_m \sec\theta)f = (\omega/\beta_1)\sec\theta = \omega/\beta \quad (2.10)$$

$$\therefore\ \beta = \beta_1 \cos\theta$$

In these equations, β is the propagation constant of the plane TEM waves in the material of the guide layer.

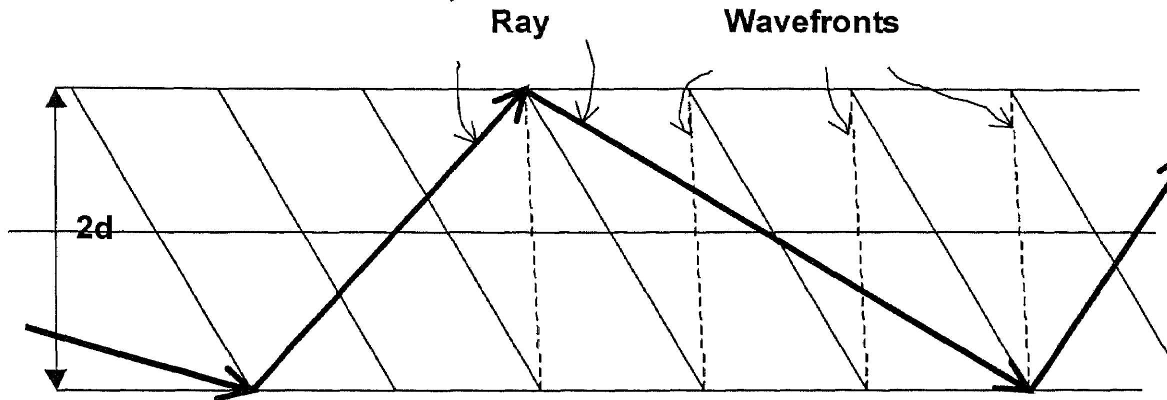

Figure 2.6 Propagation by Multiple Reflection in Planar Waveguide

As we discussed earlier the limiting angle of obliqueness, θ_m, is set by the critical angle, ϕ_c, and is given by

$$\sin \phi_c - \cos \theta_m = n_1/n_2 \quad (2.11)$$

Thus θ_m determines a minimum value for β given by

$$\beta_{min} = \beta_1 \cos \theta_m = \beta_1 \, n_2/n_1 = \beta_2 \quad (2.12)$$

This means that rays parallel to the axis have a propagation constant near to β_1, whereas the most oblique guided waves have propagation constant, β_2, which is that of plane TEM waves in the confining layers. We expect $\beta_2 < \beta < \beta_1$.

Fig 2.6 enables us to discuss another important property of the wave solution in terms of the ray model. This is the fact that only a finite number of discrete modes may propagate. In a diagram, these are represented as plane TEM waves and it is clear that if they are not to interfere destructively after multiple reflections, then the distance 2d cosec θ $(1 - \cos 2\theta) = 4d \sin \theta$ must be an integral number of wavelengths.

Thus

$$\sin \theta_i = i\lambda_m/4d = i\lambda/4n_1 d \qquad (2.13)$$

where i is an integer. Thus, only a finite number of discrete propagating angles satisfying Eq. (2.13) is permitted. Each of these corresponds to a particular waveguide mode with its own characteristic field distribution and its own propagation constant β_i, that we expect to lie between β_1 and β_2. Since $\theta_i \le \theta_m$, the number of these modes is limited to

$$M = (4\ n_1\ d/\lambda) \sin \theta_m = (4d/\lambda)(n_1^2 - n_2^2)^{1/2} \qquad (2.14)$$

Note here that the ith guided mode can propagate only if $i\lambda \le 4d\ (n_1^2 - n_2^2)^{1/2}$. At wavelengths longer than this, it is cutoff. The ith mode does not meet this condition for total internal reflection and is refracted at the dielectric interface. It does still satisfy the conditions for it to propagate freely in the confining layers and is said to be a radiation mode.

We now obtain expressions for the field distributions of the guided modes. There are two sets of guided wave modes having the form $\Psi = \Psi\ (x, y) \exp \{-j(\omega t - \beta z)\}$. These are the TE modes, in which E_z is zero, and the TM modes, in which H_z is zero. We restrict discussion to the TE modes, which satisfy the equation

$$\frac{d^2E_y}{dx^2}+\left[\frac{\omega^2 n_1^2}{c^2}-\beta^2\right]E_y=0 \tag{2.15}$$

With $n^2(x) = n_1^2$ for $-d \leq x < d$, and $n^2(x) = n_2^2$ for $x < -d$ and $x > d$. Furthermore, E_y and H_z (and hence $\partial E_y/\partial_x$) are continues at $x = \pm d$. thus, in the guide layer,

$$\frac{d^2E_y}{dx^2}+\left[\frac{\omega^2 n_1^2}{c^2}-\beta^2\right]E_y=\frac{d^2E_y}{dx^2}+u^2E_y=0 \tag{2.16}$$

And in the confining layer

$$\frac{d^2E_y}{dx^2}-\left[\beta^2-\frac{\omega^2 n_2^2}{c^2}\right]E_y=\frac{d^2E_y}{dx^2}+\omega^2E_y=0 \tag{2.17}$$

We have put

$$u^2=\omega^2 n_1^2/c^2 - \beta^2=\beta_1^2 - \beta^2 \tag{2.18}$$

and

$$w^2 = \beta^2 - \omega^2 n_2^2/c^2 = \beta^2 - \beta_2^2 \tag{2.19}$$

For the wave to be guided, it is necessary that u and v are both real. That is,

$$\beta_1^2 = \omega^2 n_1^2/c^2 > \beta^2 > \omega^2 n_2^2/c^2 = \beta_2^2 \tag{2.20}$$

These conditions mean that the solutions in the guide layer are oscillatory, while those in the confining layers decay exponentially to zero at infinity.

For there to be a guided wave solution, then, the propagation constant, β, has to lie between β_1 and β_2, as suggested by the ray model. This means that the phase velocities of the guided modes lie between $w/\beta_1 = c/n_1$ and $w/\beta_2 = c/n_2$. In particular, they cannot exceed the phase velocity of the plane TEM waves in the confining layers.

The electric field distributions for the guided modes take the form

$Ey(x) = E_s \cos ux$

$$|x| < d \qquad (2.21)$$

OR

$E_y(x) = E_a \sin ux$

and

$$E_y(x) = E_c \exp(-|wx|) \qquad (2.22)$$

$$|x| > d$$

where E_s, E_a, and E_c are constant values of electric field strength.

The number of half periods of E_y that occur in the guide layer characterizes a given mode and determines the value of u and hence the propagation characteristics of that mode.

Application of the boundary conditions at ±d enables the number of guided modes and their propagation parameters to be obtained. Consider a mode having m half-periods and therefore (m-1) zero crossings. Let its propagation be characterized by $u = u_m$, $w = w_m$. The boundary conditions require us to equate $E_y(d)$ as given by Eq. (2.21) and (2.22). And likewise to equate the two expressions for $dE_y(d)/d_x$.

Thus for the symmetric modes

$$E_y(d) = E_s \cos u_m d = E_c \exp(-w_m d) \qquad (2.23)$$

and

$$dE_y(d)/dx = -u_m E_s \sin u_m d = -w_m E_c \exp(-w_m d) \qquad (2.24)$$

Dividing Eq. (2.24) by Eq. (2.25) gives

$$w_m d = u_m d \tan u_m d \qquad (2.25)$$

The corresponding expression for the antisymmetric modes is

$$-w_m d = u_m d \cot u_m d \qquad (2.26)$$

These transcendental equations (2.25) and (2.26) may be solved graphically to provide values for u_m, w_m and hence β_m, for any given value of the parameter V, which is defined as

$$V = (u_1 + w_2)^{1/2} d = (\omega d/c)(n_1^2 - n_2^2)^{1/2} = (2\pi d/\lambda)(n_1^2 - n_2^2)^{1/2} \qquad (2.27)$$

Thus the maximum number of modes a waveguide can support is equal to the next integer greater than $2V/\pi$. In this project, we have worked with single mode waveguides.

2.4 Summary

In summary, the size and the index of refraction difference $n_1 - n_2$ determines the number of optical modes propagating in the waveguides. This is important, since we would like to operate in the spectral region where only one mode is propagating through the waveguide (single-mode waveguide). The same applies to the ring waveguide. The theory for the ring waveguide is much more complicated and out of the scope of this thesis.

CHAPTER 3

DESIGN AND MANUFACTURING OF MASKS

3.1 Introduction

The most important procedure towards the design of the resonators was the proper design of the masks. Two masks were required for the project. One mask had the drawing of the rectangular waveguides and the other mask had the drawing of the ring waveguides. The two masks were linked with each other in the sense that both waveguides needed to be properly aligned with each other. The mask for the rectangular waveguides was first designed followed by the mask for the ring waveguides. The latter was impressed on the same waveguide structure. The details of this are given below.

3.2 Mask for the Rectangular Waveguides

The mask for the rectangular waveguides was made using layer CONT2POLY. The different waveguides were arranged in a manner, which can be seen in Fig. 3.1. The dimensions of the waveguides, which vary are as follows.

As can be seen in Fig. 3.1 parameters "A" and "B" vary as follows:

1) Parameter "A": Parameter "A" varies from 2.5 μm to 4.5 μm in steps of 0.5 μm. "A" takes values 2.5, 3.0, 3.5, 4.0, 4.5.

2) Parameter "B": For every value of parameter "A", "B" takes values, which are as follows: 300, 240, 160, 100, 80, 60, 40, 20, 12,

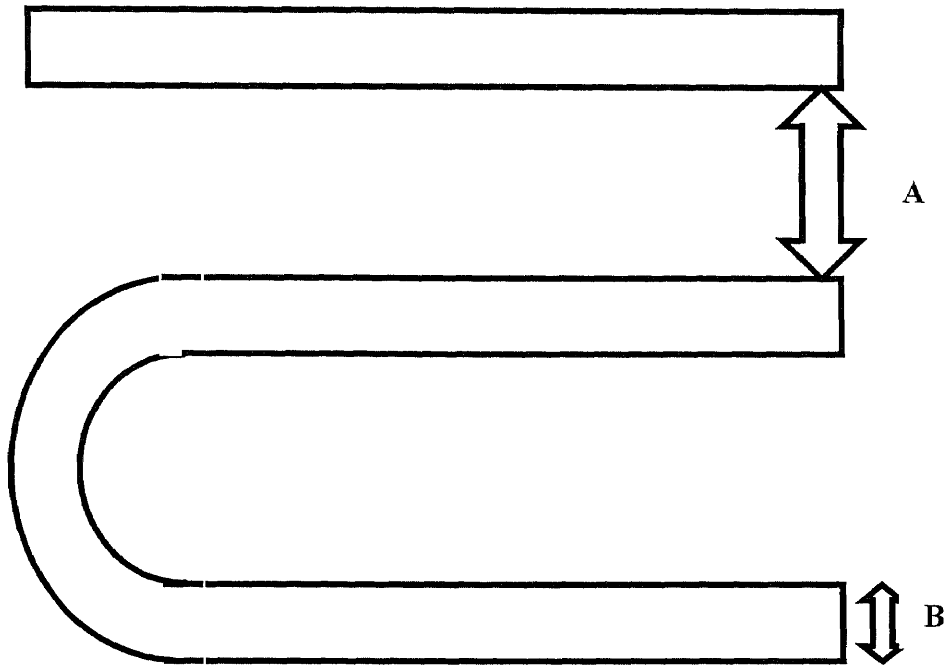

Figure 3.1 Top View of the Rectangular Waveguide

There can always be problems processing a silicon wafer. However, this generally affects only some part of the .wafer. So as a safeguard against such problems, each combination of "A" and "B" is repeated 10 times. Altogether, we have 45 different patterns on the mask. With the added redundancy there are total of 450 patterns.

The patterns were divided into different blocks as can be seen from Fig. 4.2. Each block has one pattern. As we have shown earlier, we need 450 such blocks. Each pattern in the same column has the same value of parameter "A". The value of parameter "B" varies from top to bottom. For example the pattern 1 will have "A" = 2.5 μm and "B" = 12 μm. Similarly pattern 450 will have "A" = 4.5 μm and "B" = 300 μm. There is a blank

space of 500 μm between each column. The entire structure forms a square. When placed on a 4-inch wafer, the square leaves a space of 12.5 mm from each side needed for handling. The diagram of the actual mask is shown in the Fig. 3.3.

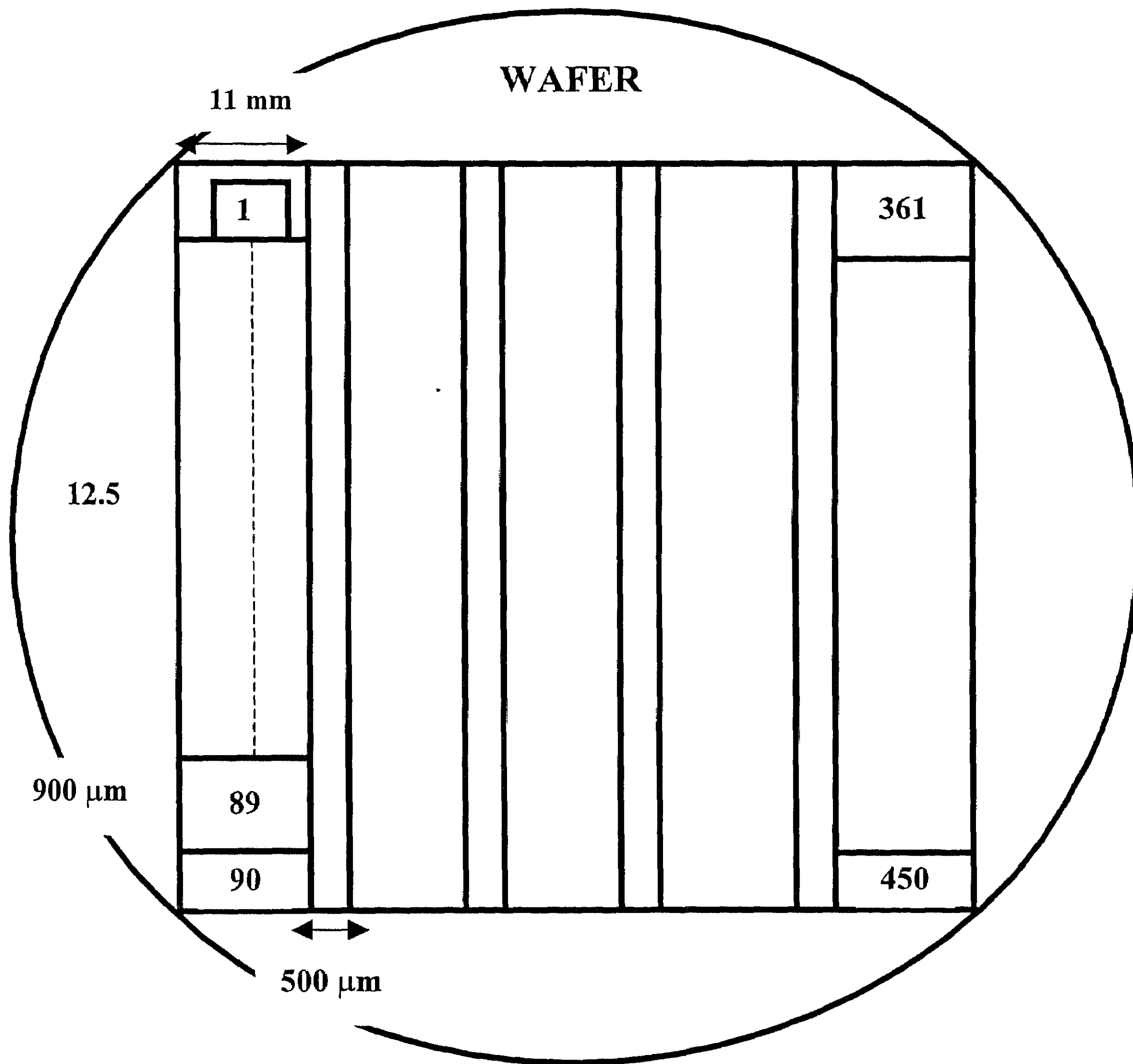

Figure 3.2 Structure and Placement of Different Patterns

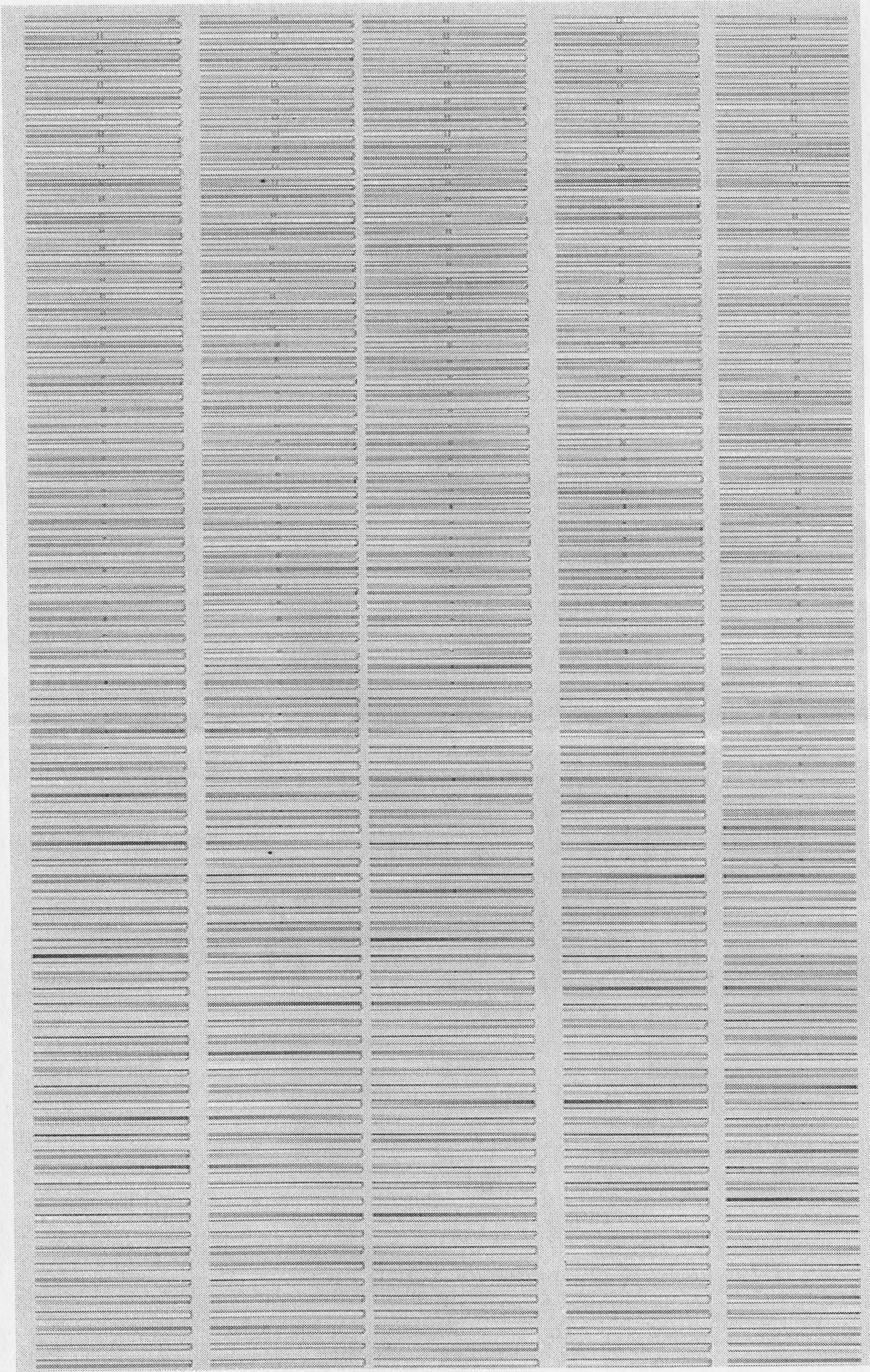

Figure 3.3 Schematic of the Final Mask

3.3 Mask for the ring waveguides

The mask for the ring waveguides was made in consideration with the mask prepared for rectangular waveguides. This has to be done to preserve the alignment between the patterns on the two masks. The exact placement of the rings can be seen from Fig. 3.4. The inner diameter of the rings is equal to the value of "A". The inner diameter is equal to value "B". This mask only consists of rings.

In Mentorgraphics, rings are drawn by changing the input mode to an arc. For making this mask the layer, CONT2ACTIVE was used. Similar to the previous mask the CMOS 1.2 μm library file was used.

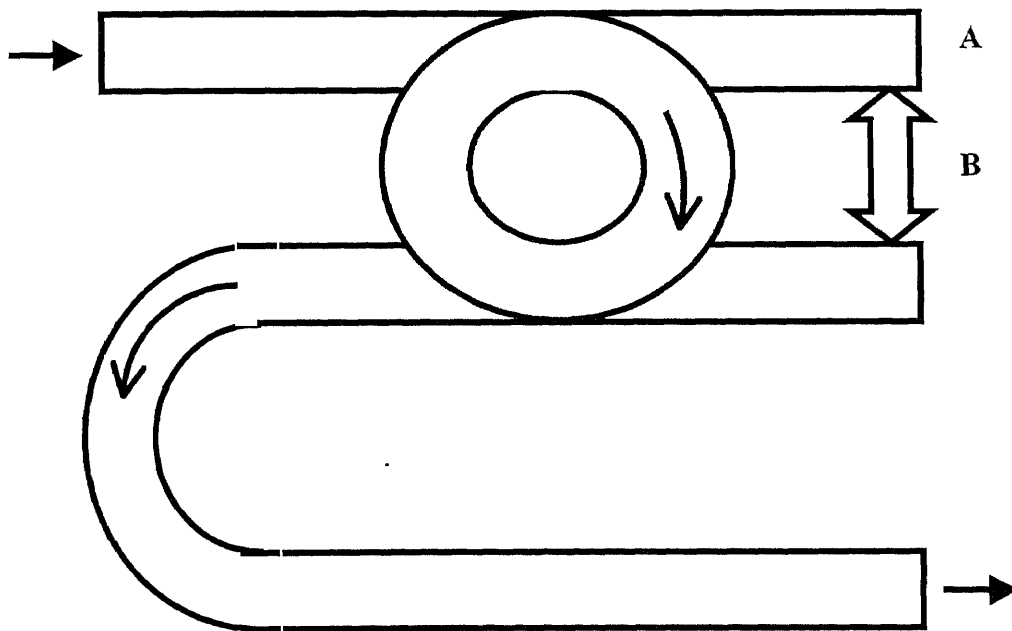

Figure 3.4 Basic Structure in the Ring Mask

Both the masks were E-beam masks, which means that the minimum pattern resolution was 0.5 μm. The E-beam type of mask is preferred over optical mask because of its superior elemental resolution.

3.4 Precautions while Making the Mask

The following paragraph enlists the different precautions to be followed while making the mask:

1) Importance of Correct Fracture Window:

   Unlike optical pattern generation data to be used in making E-beam masks must first be fractured into MEBES data. This data file defines the write area for the MEBES just like a reticle defines the exposure area for the photorepeater. The file must have physical boundaries, which are determined by a given set of co-ordinates used in the design of the device. Fig. 3.5 shows three different windows. The solid line represents the desired fracture or design window. This window encompasses the data on all layers, using a common center and extends beyond the data limits to provide definition between the data and the background of the mask on the clearfield levels. The two dotted lines represent the data limits of layer 1 and 2 respectively. If the data limits are used as a fracture window, two possible problems may arise. First since the pattern placement on the mask is determined by the center of the fracture window, the placement from layer to layer will be different if different fracture windows are used.

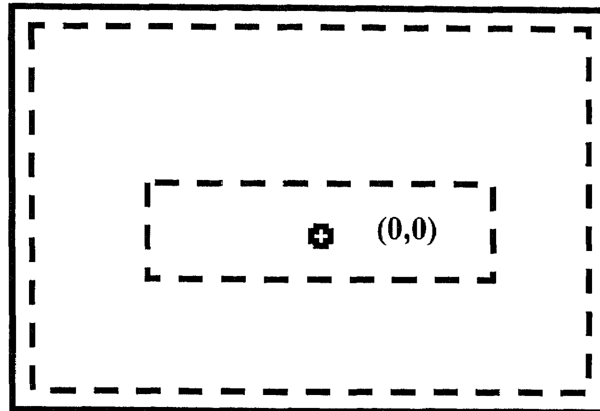

Figure 3.5 Desired Fracture Window

2) Positioning the pattern within mask limits:

It is important to keep the pattern within the limits of the window area of the mask. If the pattern is close to the edge of the window area of the mask or if touches the edge of the window, some of the pattern may spill outside the window and can cause unnecessary patterns on the mask. This can be better understood by looking at Fig. 3.6 below.

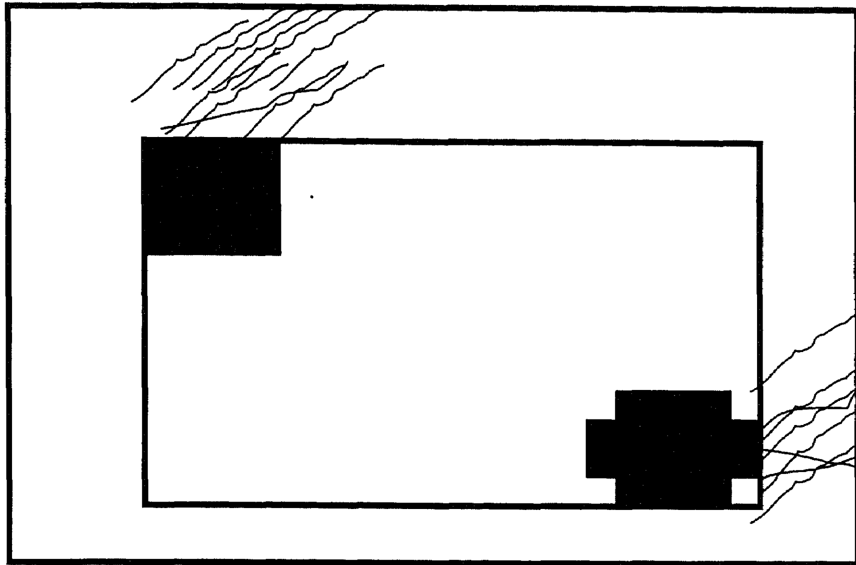

Figure 3.6 Image Spill due to Improper Positioning of Pattern

3.5 Ordering the Mask

Interfacing with the mask manufacturer is not a simple task. The mask was ordered from a company named "Photronics Inc.". The data that the company requires for processing the order is as follows:

1) The data file should be in GDS 11 format. The Mentorgraphics file can be converted into the GDS 11 format using the IC Station link in Mentorgraphics.

2) The layer which is to be used for making the mask. The mask may contain different structures, but the layers differentiate between different structures.

3) Center of the structure and the displacement of the structure from the center.

4) Co-ordinates of the endpoints of the structure.

5) The points where we may find the minimum and maximum dimensions in the structure. These are used as reference points.

6) The scale factor for the data. This means that the data may be needed to be reduced to get the right dimensions. We have used a scale factor of 0.4.

7) The type of mask needed such as E-beam. In addition, the size of the mask required like 4" or 5".

The final file is sent by FTP to the manufacturer. The manufacturer fabricates the mask according to specifications. The received mask should be opened only in a clean room with rating of at least 100.

CHAPTER 4

FABRICATION OF WAVEGUIDES

4.1 Introduction

Any work in semiconductors requires a clean room environment with highly accurate and precise equipment. Any process during the fabrication process needs to be decided in advance before it is implemented. Before beginning the actual fabrication process, a traveler for the project is created. The traveler lists in detail the different processes to be carried out for the proper execution of the project. The traveler not only acts as a guide while working on a project but is also used to record certain observations while making the project.

4.2 Process of Fabrication

The following project was done in a state of the art Class 10 cleanroom at the Microelectronics Research Center at NJIT. The fabrication of the waveguides was done using CMOS grade silicon wafers. The detailed process of fabrication is explained below.

1) The first step is to clean the wafers thoroughly using M-pyrol. M-pyrol has two baths, one primary and one secondary. The secondary solution is fresher than the primary solution. Therefore, the wafers need to be dipped first in M-pyrol solution primary, and then in the secondary, each for 10 minutes. The temperature of both the primary and secondary should be set at 95° C for best results. Then the wafers were put in distilled water for 10 minutes. The resistance of the water is checked.

The resistance is more than 5 Ω's for a clean wafer. Then the wafers are spin dried in a drier. M-pyrol removes any organic dirt present on the wafers and makes it ready for P-clean.

2) After this process the wafers are loaded into the P-clean carrier. The P-clean solution is a mixture of HF and H_2SO_4. Every morning the P-clean bath has to be dispensed with H_2SO_4 to make it effective. After dispensing, the wafers are put in the P-clean bath for 10 minutes. The bath should be at 110°C. After this the wafers are dipped in hot water (80°C) for 10 minutes and then in cold water for another 5 minutes. This is necessary to bring down the wafer temperature slowly, to prevent any harm to the wafers. P-clean removes any superfluous oxide from top of the wafer surface.

Figure 4.1 CMOS Grade Silicon Wafer before Bonding

3) After the wafer cleaning process, the wafers need to be prepared for wet oxide deposition. The process of oxidation involves the following steps:

1) Furnace pre-clean

2) HF clean

3) Depositing oxide in the wet furnace

The first two processes need to be carried out just before putting the wafers in the furnace. If the process of P-clean was carried out on the wafers on the same day, it need not be repeated. Otherwise, it has to repeated again. The process is already described in Part 1. The cleaned wafers are put in the furnace pre-clean bath for 5 minutes. Then the wafers are put in distilled water for 10 minutes. The wafers are then spin-dried. These wafers are then inserted in 100:1 HF solution for 1 minute. They are then put in water and then dried. HF solution deposits a small amount of oxide on the wafers, which helps in proper oxide deposition. The cleaned wafers are then put in a closed clean container to prevent them from being exposed to the open air, which may contain dust particles. The wet oxidation furnace is then programmed for oxide deposition. The temperature is 1100°C and time required is about 11 hours. After removing the wafers from the furnace, the thickness of the oxide is measured. The deposited oxide on both the wafers should be about least 2 μm. The process of wet oxidation has an oxide growth rate of about 0.2 μm/hour. Though it is comparatively slow, the oxide deposited is fairly uniform and of good quality, which is helpful for wafer bonding.

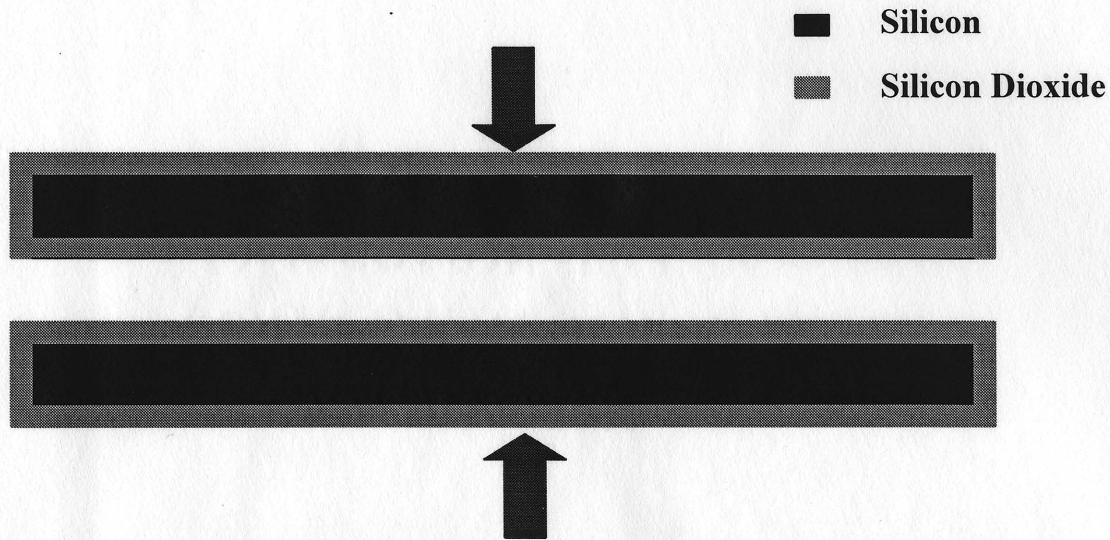

Figure 4.2 Silicon Wafers with Oxide being Bonded

4) The wafers with oxide are then bonded in a bonding machine. The force applied is 200 N for about 30 seconds. The bonded wafers are then inspected using an infrared camera. They are examined for any defects like air bubbles. Fig. 4.4 shows a bonded wafer with defects. The air bubbles trapped in between the two wafers can be clearly seen. While etching this wafer in KOH bath, some liquid can very easily creep in and break the bond.

Fig. 4.5 shows a perfectly bonded wafer. There are no striations or some other defects seen.

Figure 4.3 Bonded Silicon Wafers

Figure 4.4 Improperly Bonded Wafer. Air bubble trapped in between two wafers can be clearly seen

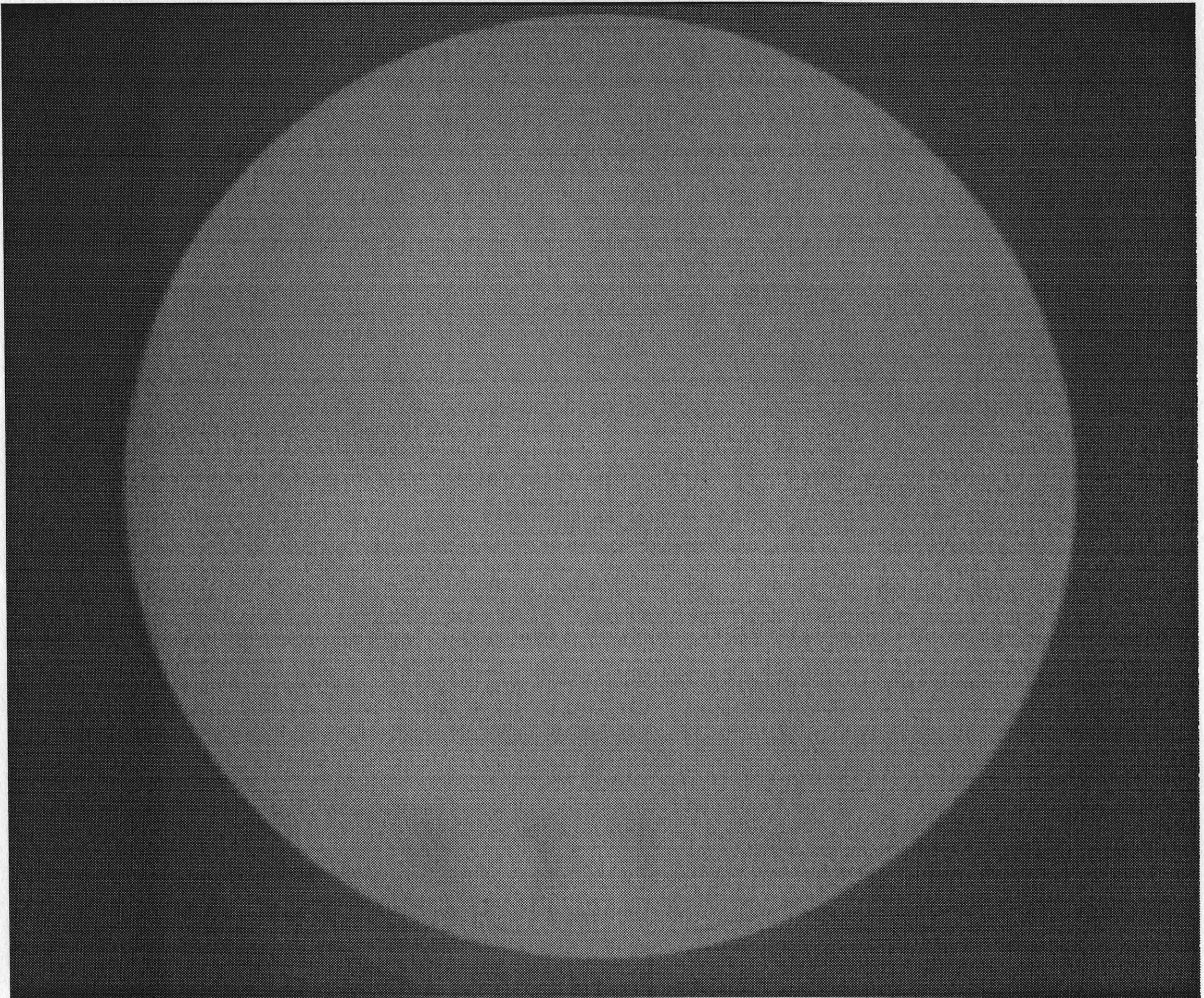

Figure 4.5 Perfectly Bonded Wafer.

4) The bonded wafers after inspection and confirmation that the bond is strong, are taken for Annealing. Annealing strengthens the bond further. It also makes the bonding uniform. Annealing is generally done out at 1100°C and carried out for about 3 hours.

5) The annealed wafers are then allowed to cool and then are prepared to deposit nitride. The pre-cleaning procedures carried for depositing oxide are also carried out for Nitride deposition. The only difference is that the bonded wafers cannot be spin-dried as this may break the bond. So everytime the wafers are dried with a Nitrogen spray. The wafers are put in the Low Temperature Nitride deposition furnace. The time is about 2 hours for 20000 Å. After removing the wafers from the furnace they are inspected and thickness of nitride is measured.

6) The bonded wafer is then taken to the photolithography room. A thick layer of photoresist is applied on both sides of the wafer. Then one side of the wafer is exposed under a mask, with a hole in the center. A black paper with a hole in the center can also be used as a mask. The exposed side of the wafer is then developed using a developer and dried. Then the wafers are etched using Phantom plasma etch. While etching, a ring with a hole in the center is placed on top of the wafer to protect the edges. The time required for etching is about 120 seconds. The wafer is visually inspected at regular intervals and checked to see if all the

nitride and oxide is etched out. Since the oxide etch can etch both oxide and nitride, the file loaded in the Phantom etch is oxide.

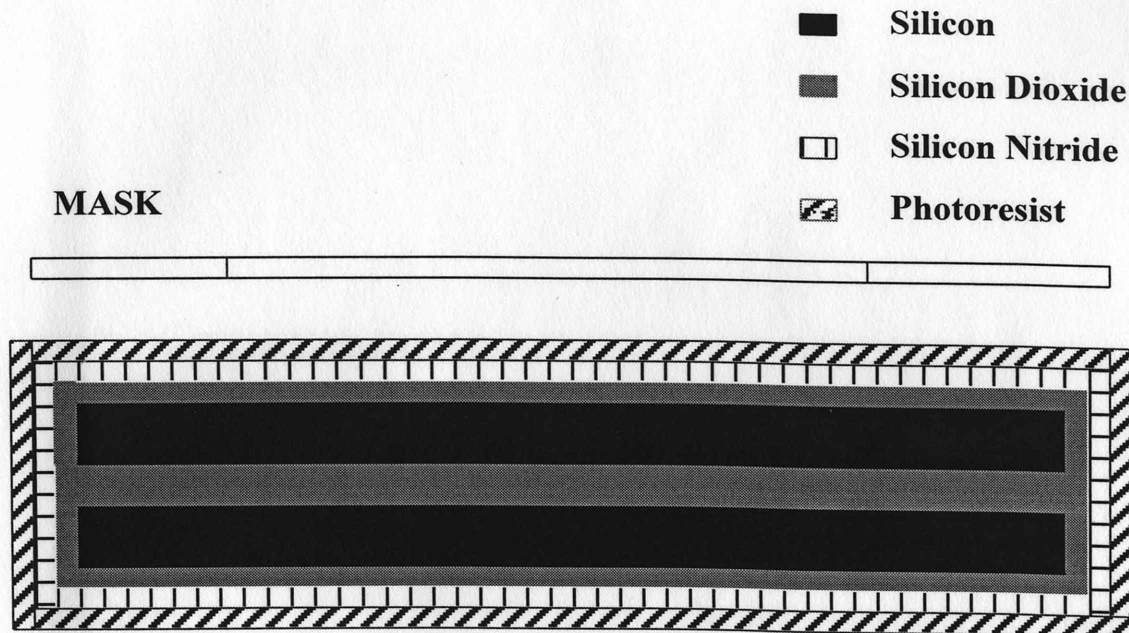

Figure 4.6 Wafer with Nitride and Coated with Photoresist

6) The wafer is then taken to the photolithography room and cleaned with acetone to remove the coated photoresist. The wafer is again visually inspected. The nitride on those parts of the wafer, which are no going to be etched, should be intact. If the Phantom etch has affected the nitride on other parts, nitride needs to be deposited again and the process repeated. Even a small exposed area can be harmful, as KOH, which is used for etching silicon, can creep through the exposed part, and damage the wafer.

Figure 4.7 Wafer, after Removing the Oxide and Nitride in the Exposure Area

8) The wafer is now ready for etching. The wafer is immersed in a KOH bath. Bubbles should be seen emanating from the exposed surface. The etch rate is about 1.2 um/sec when the KOH is fresh. It decreases, as the KOH becomes old and saturated. The etch rate also decreases are we go deep inside the silicon wafer. Periodically the wafer is removed from the KOH bath, cleaned in water and inspected. The depth of silicon etched is also measured. Initially when the depth is less, DEKTAK can be used. However, as the depth increases it is measured with a microscope. We have to etch the wafer until the thickness of silicon reaches about 2 microns. At this point, the color of the surface looks orangish, and the underlying oxide can be seen. The silicon becomes transparent. This is the point when the etching should be stopped. In addition, when the thickness of the wafer becomes about 50 microns, the wafer is etched in another bath, which contains KOH that is relatively old and saturated. This is because

with fresh KOH the etch rate is faster, but the surface of the wafer becomes rough and non-uniform. The stale KOH etches slowly but the surface stays smooth. Fig. 4.8 shows a schematic of a wafer being etched in a KOH bath.

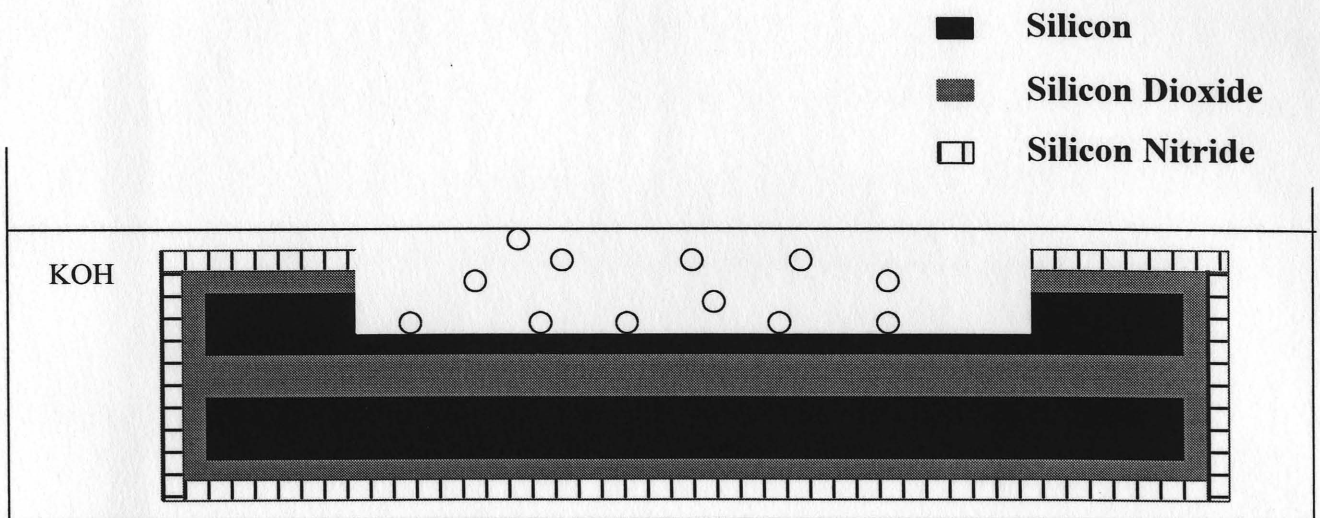

Figure 4.8 Wafer being Etched in KOH Bath

9) After the thickness of the silicon left is about 2 microns, the wafer is taken to the photolithography room. The appropriate mask is loaded on the Exposure machine. The development time is set to about 14 sec. Photoresist is applied on the wafer surface. The speed for the spinner is kept at 2500 rpm, slightly higher then the normal speed. This is done to decrease the thickness of the photoresist, as the pattern on the mask is small. The wafer is then kept on a hot plate for 1 minute and then on the cooling plate for 1 minute. The wafer is then exposed with the Hard Contact option on the exposure machine set. The exposed wafer is then kept on the spinner. Some developer is sprayed on the wafer. After a half-minute wait, some more developer is

applied. After one minute, the developer is removed by spinning the wafer and applying spraying some water. The pattern on the wafer is then observed under a microscope. If the pattern is proper, the depth of the photoresist is measured with DEKTAK. Fig. 4.10 shows one such profile. The profile of the pattern given by the DEKTAK gives an idea of the shape of the pattern. When the wafer is etched using Phantom plasma etch to get the pattern, some photoresist is also consumed. We want the depth of the pattern on the wafer to be at least 2 microns, and we could end up etching the pattern itself. So the depth of the photoresist should be at least 0.7 microns. Fig. 5.11 shows a profile after etching. It can clearly be seen from the profile, that the wafer has been etched.

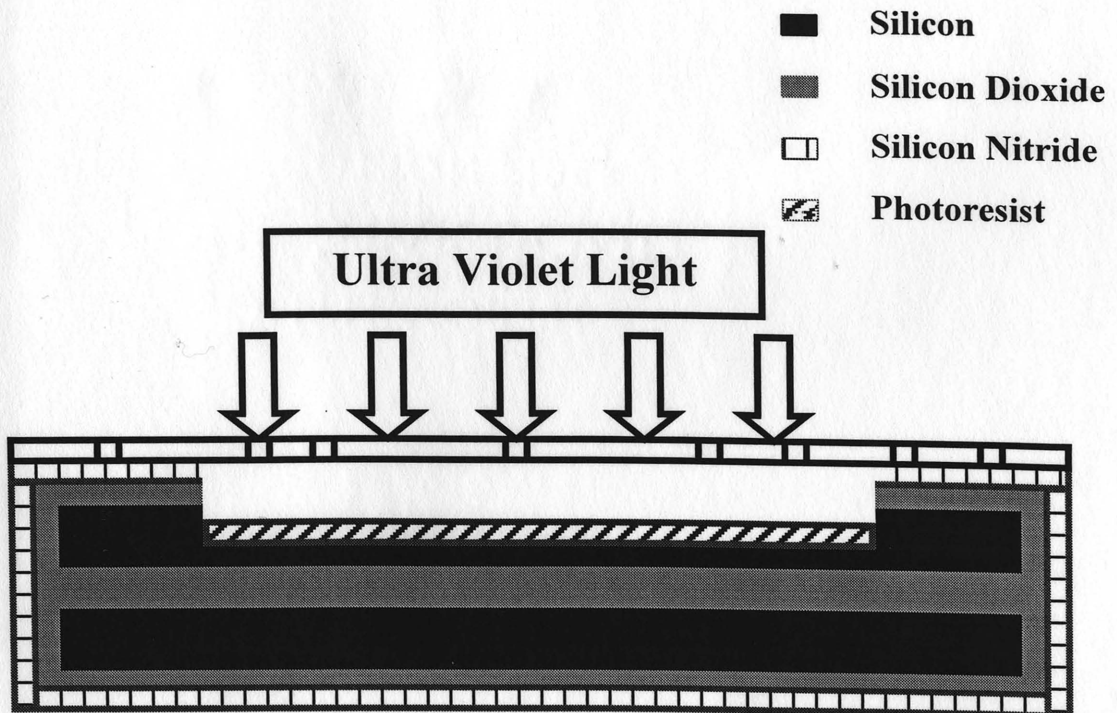

Figure 4.9 Wafer being Exposed to UV Rays

10) After it is confirmed that the pattern is true to the specification, the wafer is put in the Phantom plasma etch. The process file is set to Silica. The wafer etch time is set to 120 sec. The profile of the pattern on the wafer is regularly inspected with DEKTAK. After the depth of the pattern is as required, the photoresist on the wafer is removed using M-pyrol. The M-pyrol process is described in Step 1. The wafer is then inspected with DEKTAK.

Silicon
Silicon Dioxide
Silicon Nitride
Photoresist

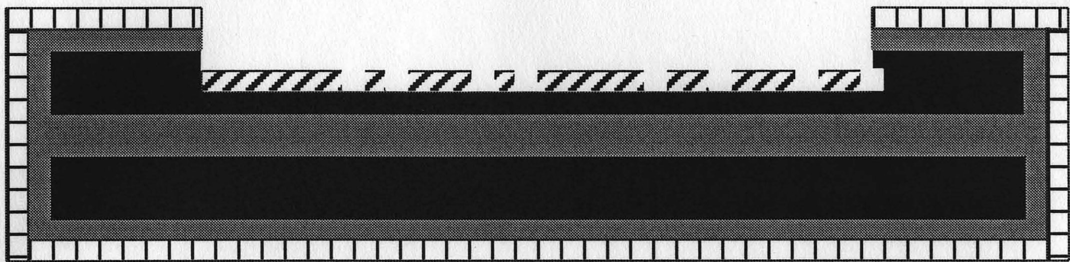

Figure 4.10 Wafer with Photoresist before M-pyrol

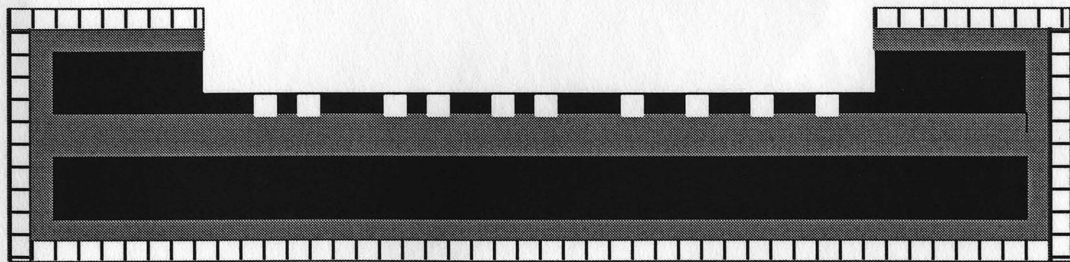

Figure 4.11 Wafer after Removal of Photoresist by M-pyrol

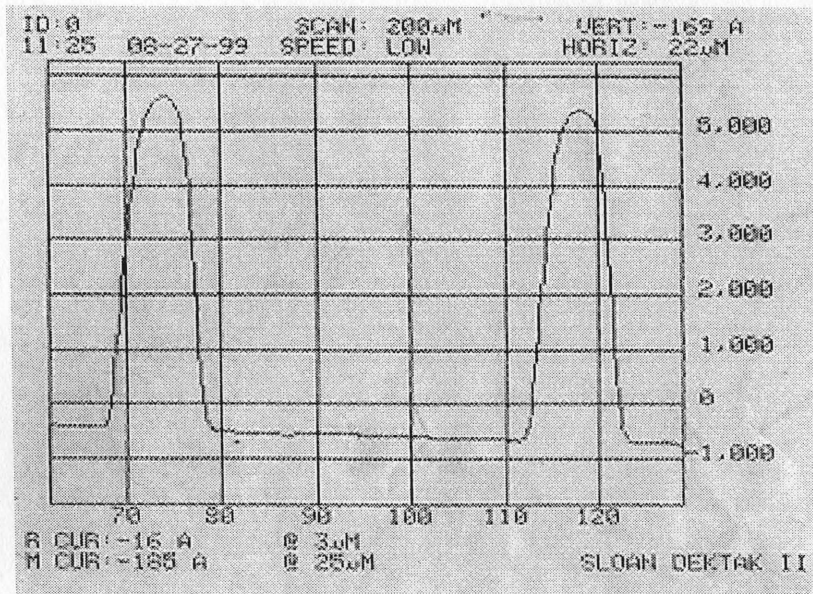

a)

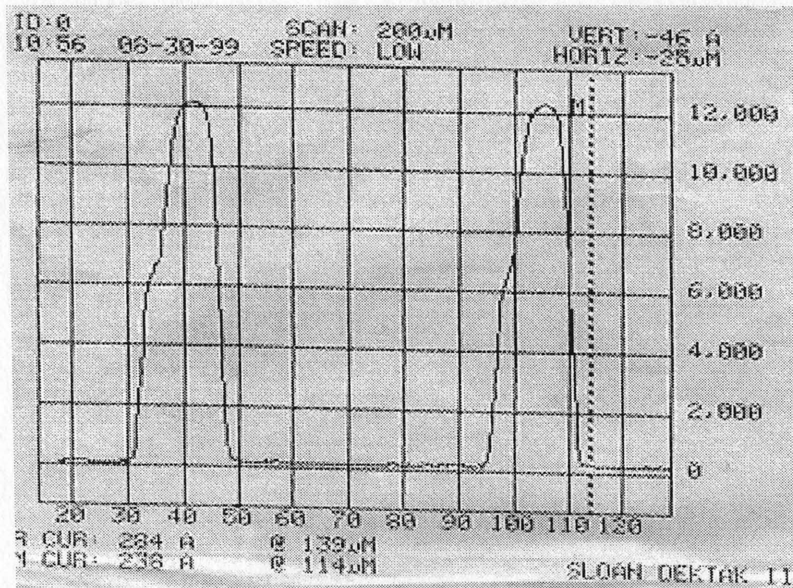

b)

Figure 4.12 a) The surface profile of the wafer measured with a DEKTAK before etching. The height of the pattern seen is equal to the height of the photoresist.

b) Similarly measured profile after etching. The height of the pattern is equal to the height of the photoresist and the depth of the silicon etched.

11) The wafer now needs to be deposited with oxide. The wafer is cleaned and all pre-cleaning processes described in Step 2 are repeated. The wafer is then placed in the Low Temperature Oxide furnace (LTO). The time required is about 2 hours for an oxide thickness of about 2.5 microns. The thickness of the oxide is then measured.

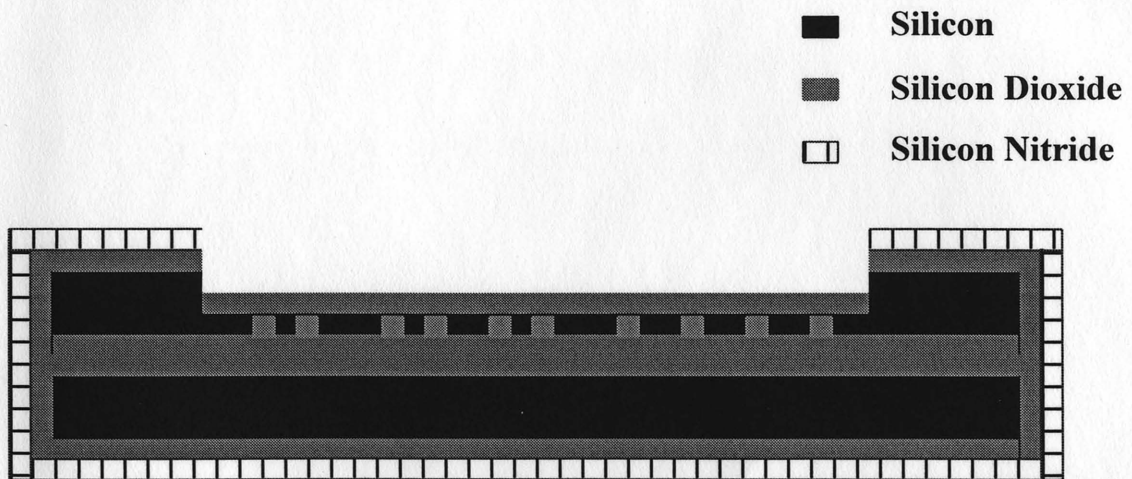

Figure 4.13 Final Wafer with Oxide

12) The above procedure is repeated for another pair of wafers. In this case the second mask is used. The first mask has a pattern for rectangular waveguides. The second mask has a pattern for ring waveguides.

Each wafer now is cut using a proper procedure to separate one or a group of waveguides. The wafers then need to be aligned and bonded together using a bonder. The wafer is now ready for measurement.

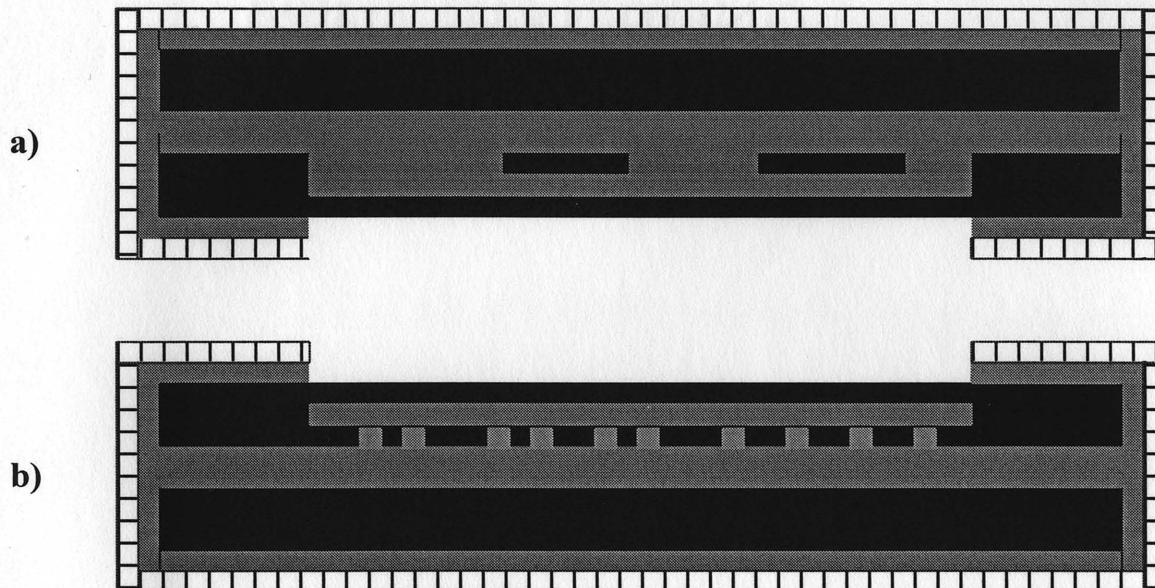

Figure 4.14 a) Wafer with Ring Waveguides b) Wafer with Ring Waveguides. Wafers can either be bonded directly or individual patterns are seperated and bonded as shown below

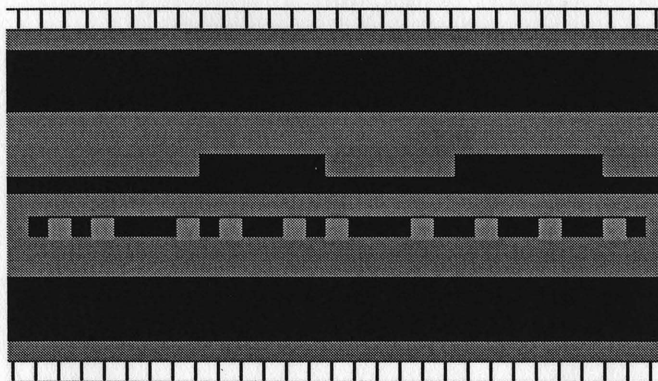

Figure 4.15 Wafers after Bonding. The resulting pattern is a resonator.

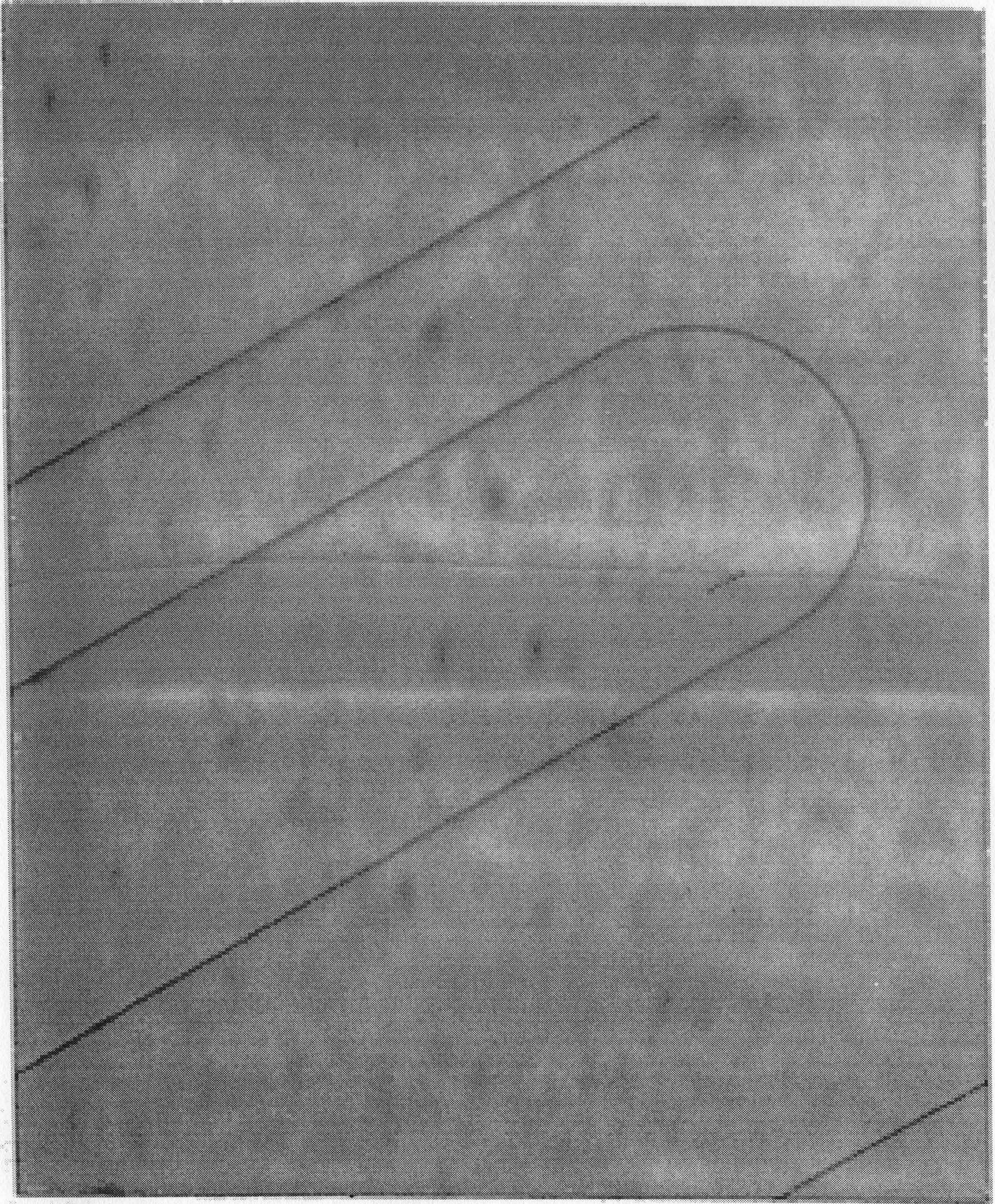

Figure 4.16 Photo of the Waveguide taken through a Microscope

CHAPTER 5

EXPERIMENTAL RESULTS

5.1 Introduction

Some experimental analysis was done on the waveguides for measuring the transmission through the waveguide. Detailed analysis of the properties and quality of these resonators has been kept for the future.

5.2 Experimental Results

1) An experiment was done on the rectangular waveguide in the resonator using laser light. Fig. 5.1 shows the experimental setup for this experiment. A single mode fiber was used to launch light into the waveguide. The output from the waveguide was taken out using a multi-mode fiber to ensure collection of output light. Then the input and output fibers were adjusted to achieve maximum signal output. The input fiber was scanned across the waveguide input and the output signal has been recorded.

2) Fig. 5.3 shows the graph of the signal output from the fiber as a function of horizontal displacement. It shows the drop and bus waveguides. Similarly, Fig. 5.4 shows the graph of the output from the fiber as a function of vertical displacement. It shows that the waveguide width is rather narrow.

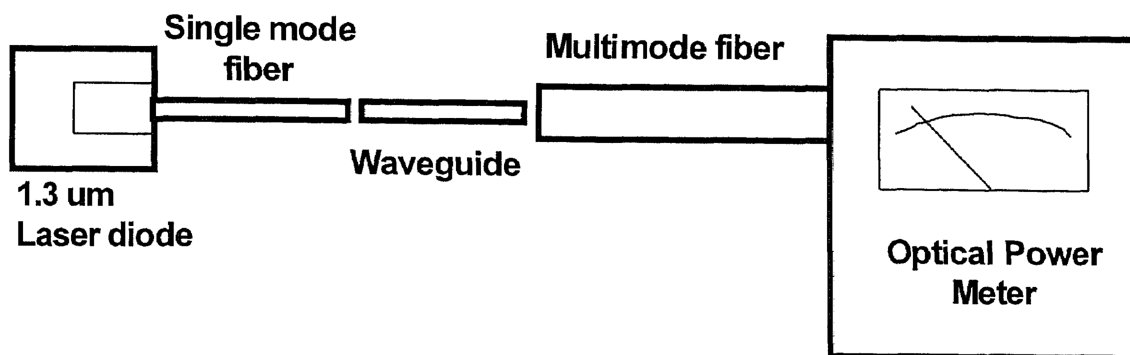

Figure 5.1 Experimental setup for measurements of transmission characteristics of waveguide

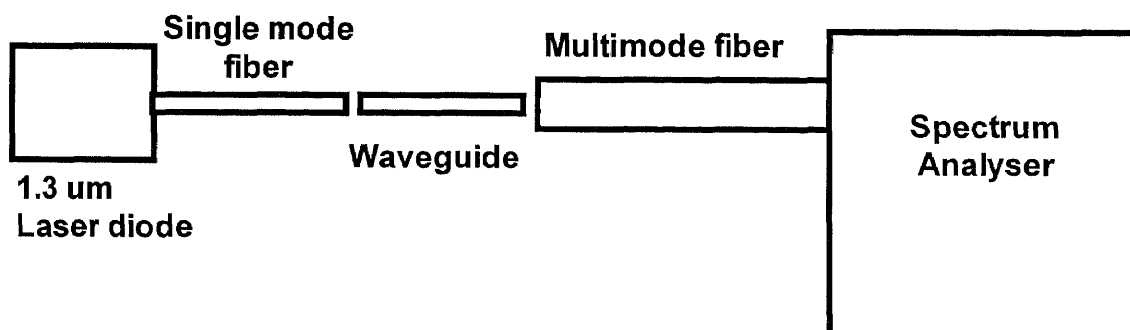

Figure 5.2 Experimental Setup for Verification of the Spectral Output of the Laser Diode

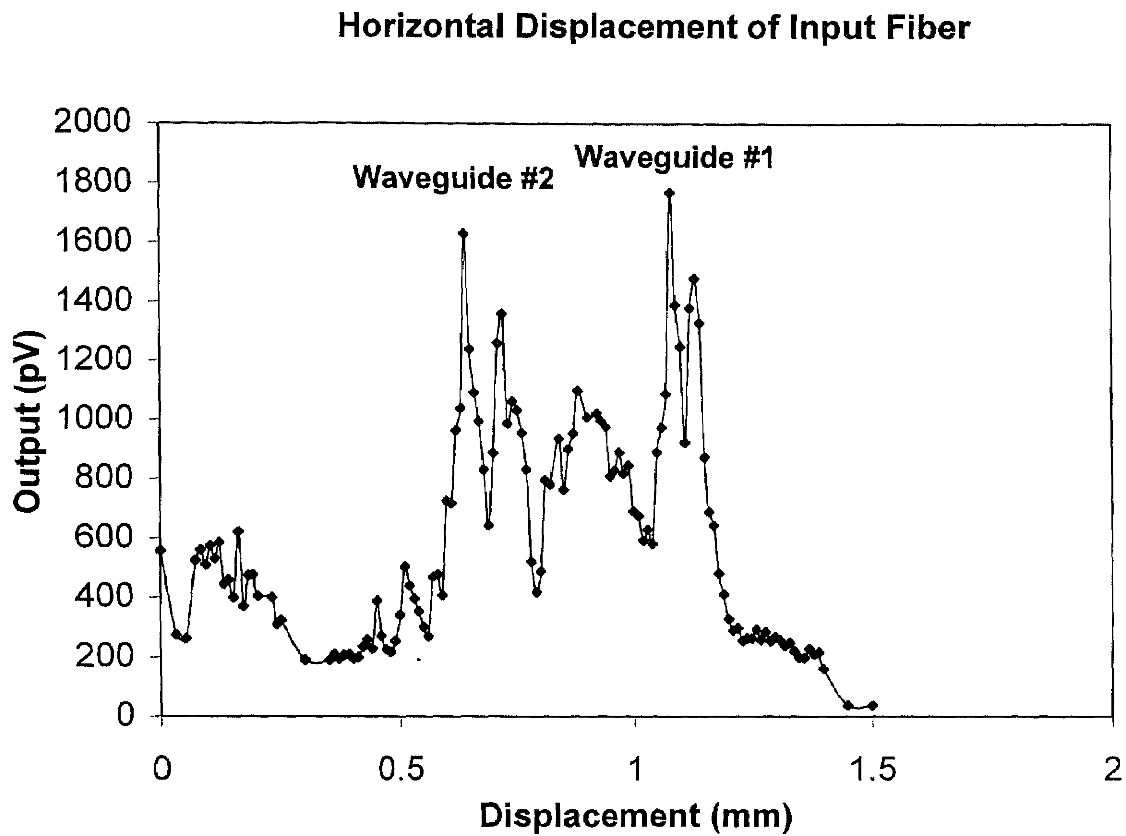

Figure 5.3 Output Profile for Laser Light as Input and Horizontal Displacement of Input Launching Fiber

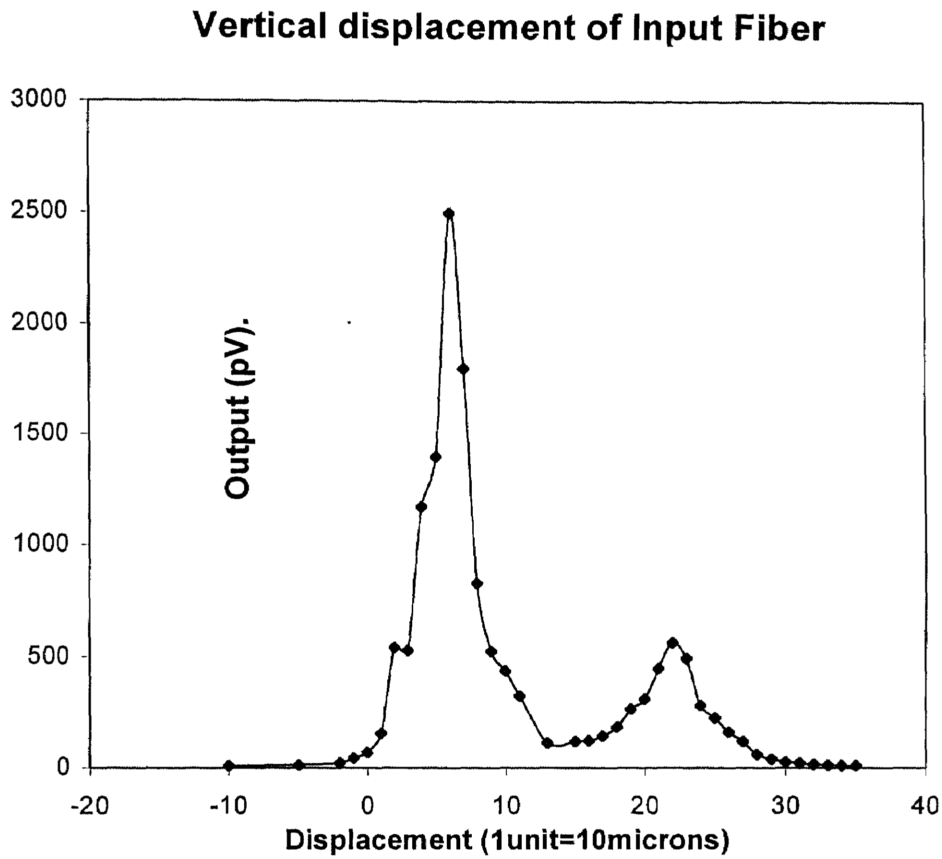

Figure 5.4 Output Profile for Laser Light as Input and Vertical Displacement of Input Launching Fiber

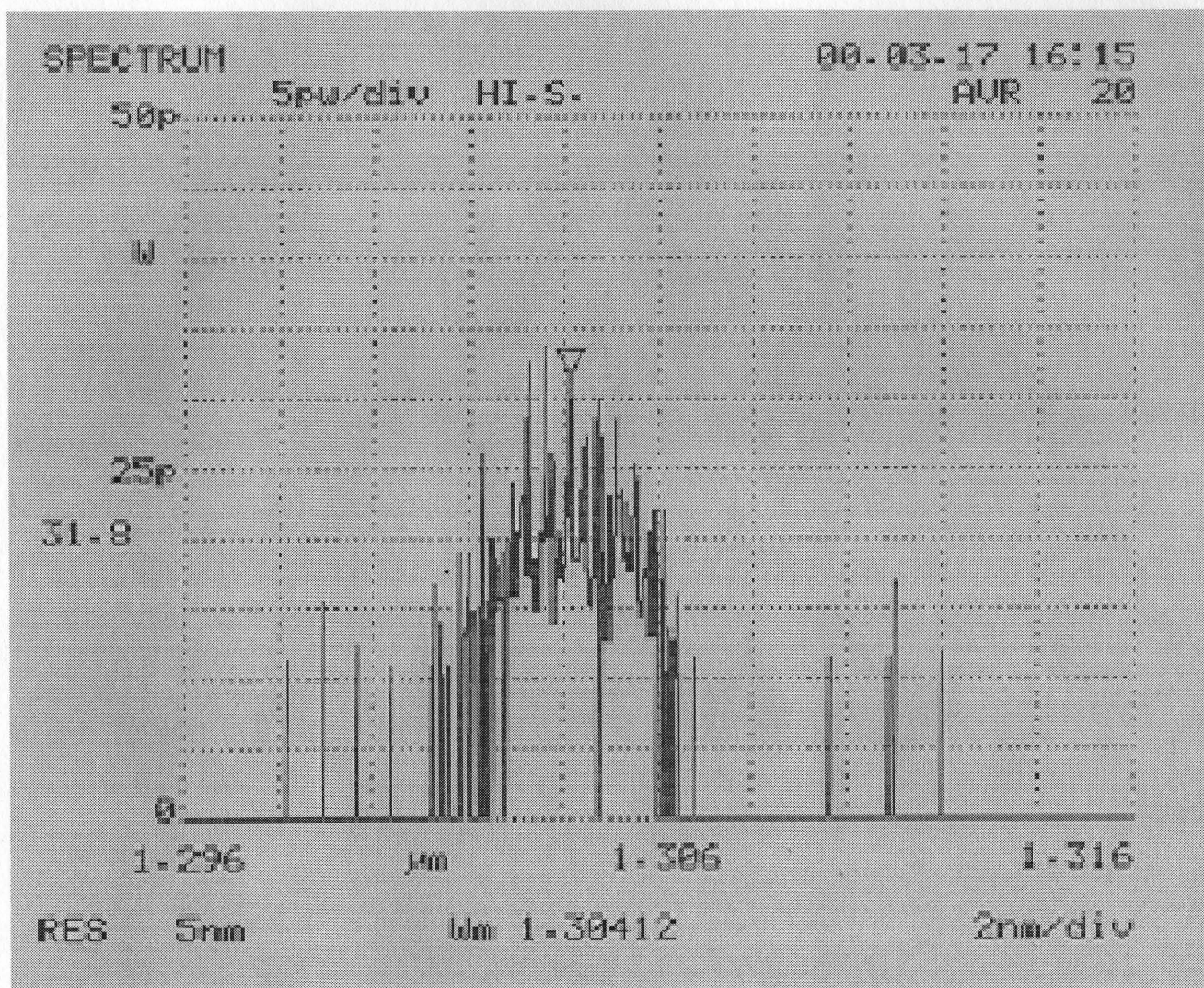

Figure 5.5 Transmission Profile for the Waveguide for Different Wavelengths indicating that the output indeed belongs to an 1.3 μm diode-laser's spectral line

3) By inspecting Fig. 5.5 we determined that that waveguide output corresponds to the laser light at $\lambda = 1.3$ μm. The experimental setup for measuring such an output is shown in Figure 5.2. Here we coupled the waveguide output to the multimode fiber, which in turn was coupled to a spectrum analyzer instead of a power meter.

4) In another experiment wherein, white light was used as the source, we tried to determine the spectral dependence of the waveguide output. The white light was passed through a wavelength selective filter. Its output was passed through a lens to focus the monochromatic light on the waveguide core. The monochromator output was measured with a Ge. detector. A pinhole was used before the Ge. detector to increase the accuracy of measurement.

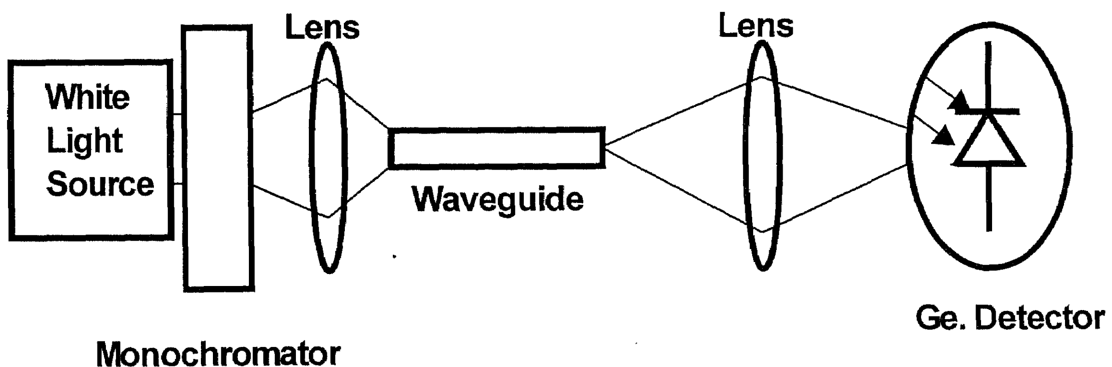

Figure 5.6 Experimental Setup for Measurement of the Spectral Characteristics of the Waveguide

Fig. 5.7 shows the output of such an experiment for measuring the spectral response of the fiber.

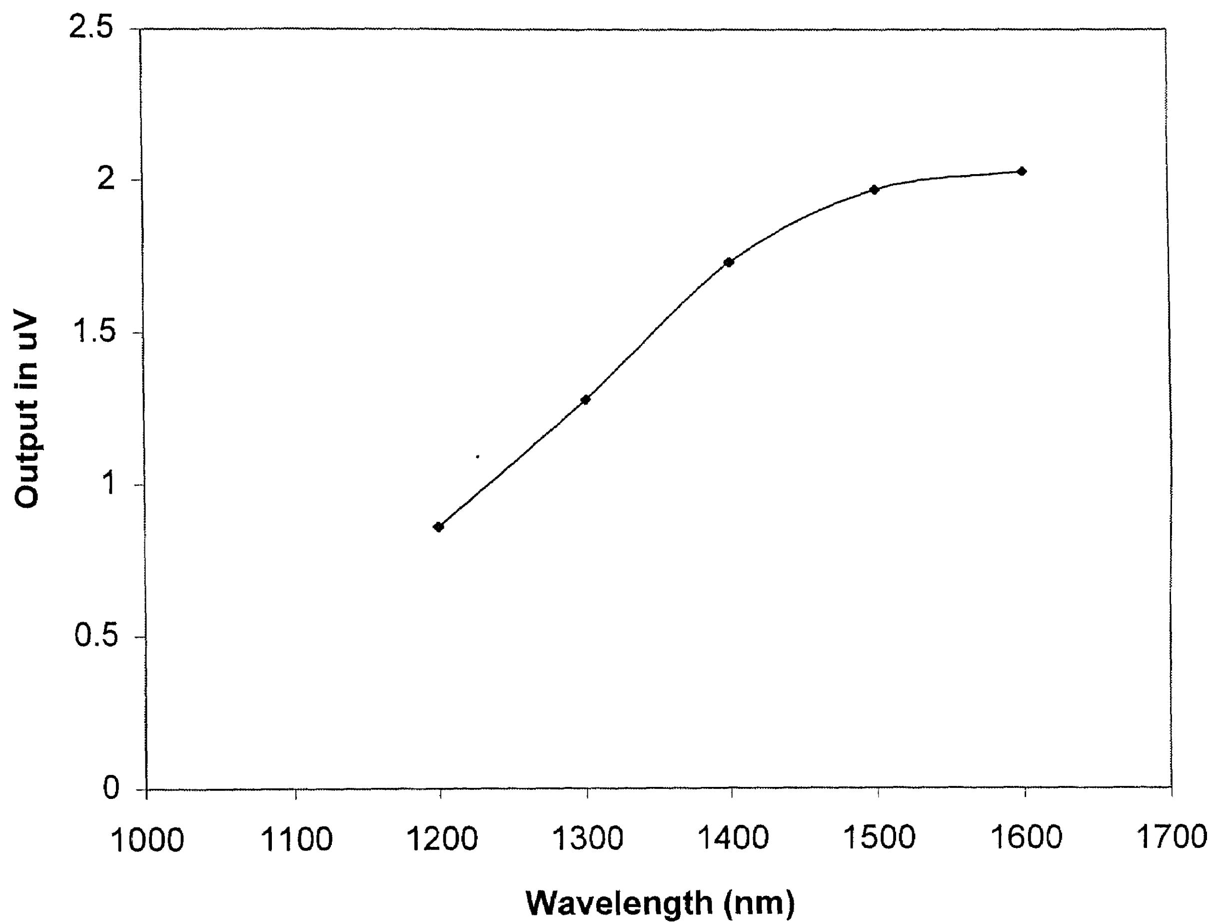

Figure 5.7 Transmission Characteristics of Rectangular waveguide with respect to Wavelength

CHAPTER 6

CONCLUSION AND FUTURE DEVELOPMENTS

6.1 Conclusion

From the observations so far, we conclude that, wafer bonding can be a very efficient method of manufacturing integrated optical multiplexer/demultiplexers. We can also conclude that silicon is a very suitable material for making such structures. The use of VLSI technologies in fabricating optical elements may therefore advance the area of optical networking and sensing.

6.2 Future Developments

A number of additions can be made to the basic resonator structure. Some of these improvements are discussed below.

6.3 Multiple Ring Structure for Better Spectral Filtering

In our project, we used ring waveguide as a resonant filter. In such a geometry, the forward propagating wave in the bus excites a rotating mode in the ring, which in turn couples into the backward propagating mode in the drop. Ideally, at resonance, 100% transfer can be achieved. However, radiation losses and bending losses inside the ring have the effect of reducing the transfer efficiency. Furthermore, the ring waveguides supports multiple resonances.

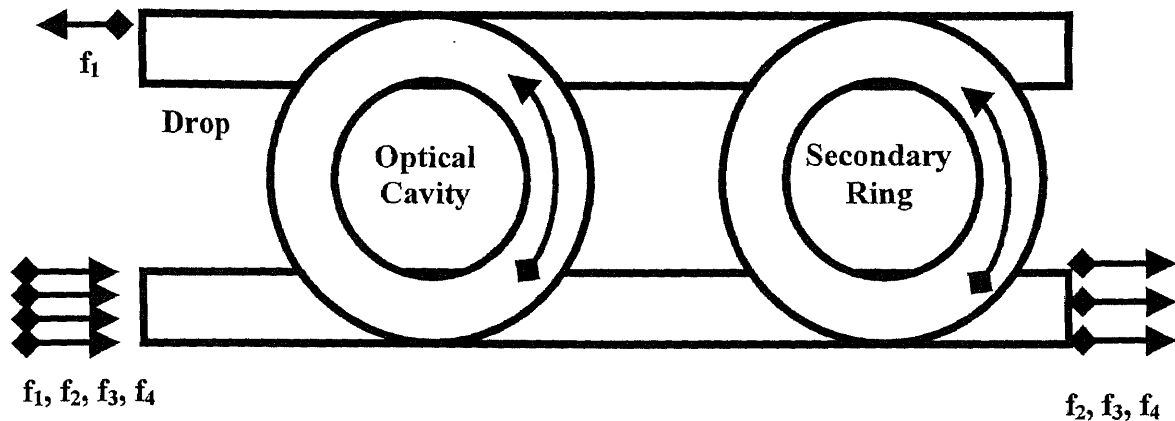

Figure 5.8 Multiple Ring Structure for Better Spectral Filtering

A multiple-ring design can also be used to increase the free spectral range, which measures the mode spacing between the frequency channels. Each ring has a different radius, and supports a different set of resonant frequencies. Maximum transfer occurs only when the resonant frequencies of both rings match with each other. Although the multiple ring geometry can increase the free spectral range of the CDF, the transfer efficiency suffers severe reduction.

In addition to the multimode nature of a ring cavity, the quality factor is limited by intrinsic radiation losses and degrades significantly with even a moderate amount of surface roughness. It is therefore of great practical interest to explore the possibilities of using photonic crystal microcavities in a channel drop filter.

REFERENCES

1. B. E. Little, S. T. Chu, W. Pan, D. Ripin, T. Kaneko, Y. Kokubun, and E. Ippen, "Vertically Coupled Glass Microring Resonator Channel Dropping Filters", *IEEE Photonics Technology Letters*, vol. 11, no. 2, Feb 1999.

2. H. A. Haus and Y. Lai, "Narrow-band optical channel-dropping filter", *J. Lightwave Technology* 10, 57 (1992).

3. B. E. Little, S. T. Chu, H. A. Haus, J. Foresi, and J. P. Laine, "Microring resonator channel dropping filters", *J. Lightwave Technology* 15, 998 (1997).

4. A. D. Chaudhari, L. C. West, C. W. Roberts, and X. Lu, "Highly compact optical waveguides with a novel pedestal geometry," IEEE Photonics Technology Letters, vol. 7, pp. 526–528, May 1995.

5. B. E. Little, J. Foresi, H. A. Haus, E. P. Ippen, W. Greene, and S. T. Chu, "Ultra-compact Si/SiO2 micro-ring resonator channel dropping filter", *IEEE Photonics Technology Letters*, vol. 10, pp. 549–551, Apr. 1998.

6. F. Heismann, K. Okamoto, and M. K. Smit, "Introduction to the issue on Integrated Optics", *IEEE Journal of Selected Topics in Quantum Electronics*, vol. 2, no. 2, June 1996.

7. S. Fan, P. R. Villeneuve, J. D. Joannopoulos, H. A. Haus, "Channel drop filters in photonic crystals", *Optics Express*, vol. 3, no. 1, July 1998.

8. J. M. Senior, "Optical Fiber Communication", *Prentice-Hall International*, Second Edition 1996.

9. J. Gowar, "Optical Communication Systems", *Prentice-Hall International*, Second Edition 1995.